Unit Connected Generator with Diode Valve Rectifier Scheme

by

Sumrit HUNGSASUTRA

A thesis
presented to the University of Manitoba
in partial fulfillment of the
requirements for the degree of
Master of Science
in
Department of Electrical Engineering

Winnipeg, Manitoba

ISBN 0-315-37221-4

UNIT CONNECTED GENERATOR WITH DIODE VALVE RECTIFIER SCHEME

by

SUMRIT HUNGSASUTRA

A thesis submitted to the Faculty of Graduate Studies of
the University of Manitoba in partial fulfillment of the requirements
of the degree of

MASTER OF SCIENCE

ABSTRACT

HVDC transmission with diode bridge rectifier scheme was comprehensively studied for the case of an isolated generator source. System transfer function, which can be considered as a combination of the machine and the converter transfer function, was analyzed. The system was compensated to obtain better performance and higher stability by a lead compensator. The system was practically implemented on the HVDC simulator at the University of Manitoba for verifying the performance with different protection schemes. Digital simulation with the EMTDC program was also performed to compare the results with those achieved from analog simulation. The system was able to recover from a fault within about 1.5 second as can be seen from the results.

ACKNOWLEDGEMENTS

The author gratefully acknowledge the efforts of Dr. R.M. Mathur and Dr. R.W. Menzies for their creative initiations and guidance for this topic. The useful and stimulative guidance of Dr.A.M. Gole for using the EMTDC program in digital simulation was also appreciated. Cooperation and suggestions from the technicians at the department of electrical engineering were also appreciated. Finally, the author expresses gratitude to the Canadian International Development Agency for their financial support and a successful linkage program between the University of Manitoba and Khon Kaen University, Thailand.

NOMENCLATURE

Eo	electromotive force
E	terminal phase voltage
Ef	applied field voltage
Ed	direct axis component of E
Eq	quadrature axis component of E
U	voltage behind subtransient reactance per phase
Ud	direct axis component of U
Uq	quadrature axis component of U
Uo	voltage U under constant speed per phase
Udo	direct axis component of Uo
Uqo	quadrature axis component of Uo
I	armature fundamental current
Id	direct axis component of I
Iq	quadrature axis component of I
Idc	dc link current
X	inverter commutation reactance
Xc	rectifier commutation reactance
X_T	transformer leakage reactance
Xd	direct axis synchronous reactance
Xd'	direct axis transient reactance
Xd"	direct axis subtransient reactance
Xmd	direct axis magnetizing reactance

Xq	quadrature axis synchronous reactance
Xq"	quadrature axis subtransient reactance
Td'	direct axis short circuit time constant
Tdo'	direct axis open circuit time constant
Tdo"	direct open circuit subtransient time constant
Tkd	direct axis damper leakage time constant
ψd	direct axis flux linkage
ψq	quadrature axis flux linkage
δ	small variation
Δ	relative change (per unit change)
p	Laplace operator

LIST OF FIGURES

CONTENTS

Chapter I

INTRODUCTION

1.1 GENERAL BACKGROUND

In industrialized countries, the need of increasing energy resources is essential. Among many resources, hydro-energy is the most economical one. Unfortunately, normally these resources are located far away from the load centers.

HVDC transmission offers an opportunity to transmit economically a large amount of electrical energy over a long distance and thus allows efficient utilization of remote hydro-energy.

Nowadays, many HVDC transmission systems are in operation in many parts of the world. In those conventional systems, thyristor valves ,which are quite expensive, are employed in both inverter and rectifier converter stations. Therefore, the cost of HVDC systems depends significantly on the cost of the thyristor valves. Many authors [3],[7] have shown that the cost of HVDC rectifier station would be reduced if diode valve rectifiers were used instead of thyristor valves. However, there are still unanswered questions with regard to the operation of diode rectifiers, and their unit connection with hydro generators needs investigation.

1.2 BASIC IDEAS

The idea of replacing the thyristors by diodes at the rectifier converter station has been considered in the past [3]. In the conventional systems, the rectifier is normally operated in a constant current control mode to limit the current flowing in the valves while the inverter is operated to regulate the voltage in the minimum extinction angle control mode. This mode of operation gives the highest dc voltage and minimizes the reactive power consumption at the inverter. The control characteristic of this normal operation is shown in Fig.1.1 (a).

However, in the case that the voltage at the rectifier is reduced below the level required for marginal control at the inverter, the control action is reversed. The voltage control is transfered to the rectifier by limiting the firing angle to the minimum value, while the current control is taken over by the inverter. The control characteristic of this condition is shown in Fig.1.1 (b).

It can be perceived that in inverter current control mode, the rectifier operates virtually as a simple diode rectifier. If the thyristors are replaced by diodes at the rectifier station the control characteristic of this configuration will be as shown in Fig.1.1 (c).

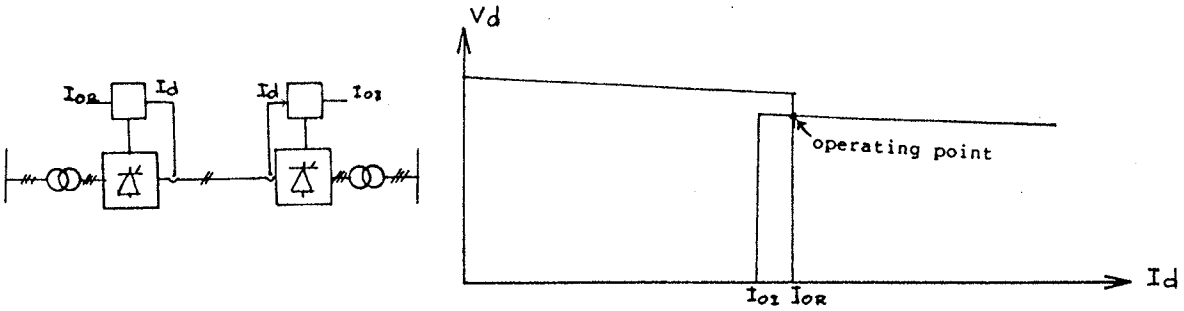

(a) Rectifier current control mode

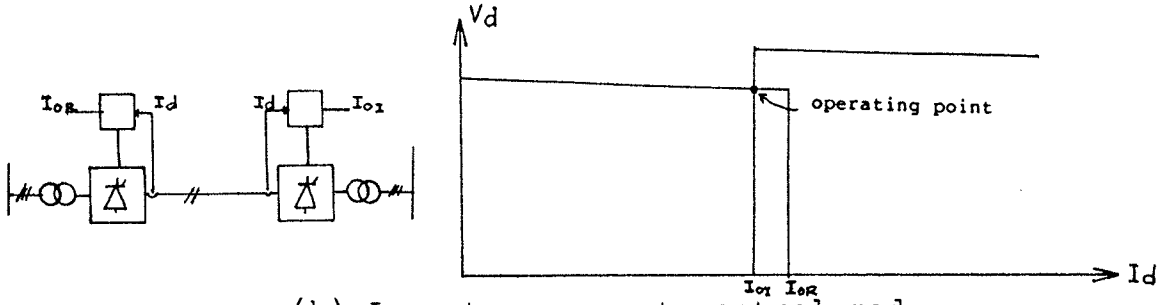

(b) Inverter current control mode

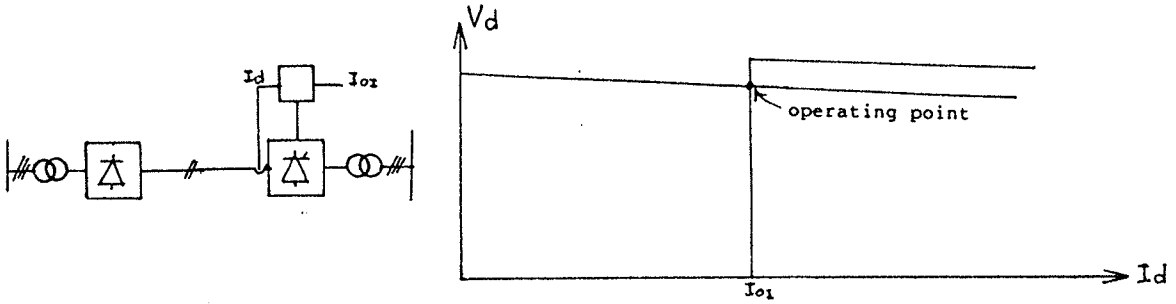

(c) Diode rectifier - inverter current control

Figure 1.1: HVDC Transmission control characteristics

1.3 PUBLISHED RESULTS

Leading researchers in this area, namely, J.P.Bowles[3], T.Machida[6], M.Hausler[7] et al, gave some advantageous conclusions and developed basic control and protection methods for this scheme.

The advantages and disadvantages of this scheme are summarized below :

Advantages of using diode rectifiers

1. Cost of the diode valve rectifier is lower.
2. There is no need of firing pulse control at the rectifier.
3. Diode elements have higher overload capability.
4. The maintenance at the rectifier is easier.
5. Reactive power required at the rectifier is reduced. Also there is no need for harmonic filters if a 12 pulse configuration of the rectifier is used.
6. Larger frequency swings are tolerable due to the absence of filters.
7. Series and parallel connection of diode rectifier units is easier. This is a very attractive feature when a multi-terminal scheme is to be used.

Advantages of using unit connection

1. Generator, transformer and rectifier can be connected together as a block unit reducing the space required.
2. In a unit connection scheme, the ac busbar is eliminated. As well, there is no requirement to run all generators in synchronism. The removal of the ac busbar limits the magnitude of fault current at the generator, transformer and switches leading to reduced cost of generators, transformers and protective devices.

3. The hydro turbines driving the generators can be run at their optimum speed corresponding to the load requirements in order to maximize the efficiency of generation.

Disadvantages

There are several disadvantages which may have precluded the application of diode rectifier until now.

1. The voltage at the sending end can not be reversed, therefore , power reversal is not possible. This may not be a serious drawback when diode rectifiers are used at the dedicated sending end of power. However, the absence of the feature makes the dc line fault clearing slow.
2. The only way to control the rectifier converter station is by means of excitation control at the generator, which is much slower. It critically depends on the ceiling voltage of the exciter.
3. Recovery from faults is very slow and may therefore be unacceptable.
4. The need for ac or dc breakers increases the cost of the system.
5. If the inverter has to operate in the constant current control mode, the reactive power consumed by the inverter is increased. This increases the Mvar rating of the synchronous condenser and filters at the inverter.

1.4 THE PURPOSE OF THE THESIS

It is proposed to perform a systematic study of the performance of diode bridge rectifiers in unit connection with turbine-generators. One of the principal concerns in the application of diode bridge converters is the difficulty of fault clearance on the dc line and system recovery. This study seeks improvements in the control action and to reaffirm the applicability of unit connected diode rectifiers to economically transmit power from remote hydro stations. Such an arrangement can be applied very efficiently to harness energy from mini hydro plants transmitted on a monopolar dc line using ground return.

1.4.1 Scope of the thesis

In order to develop a suitable protection scheme, at first a suitable transfer function of a unit connected diode bridge rectifier-generator is developed (Chapter II). The performance of the system is evaluated and a lead compensator is designed to improve the system response (Chapter III). In Chapter IV various protection and control schemes are examined, and suitable controllers are designed. To determine the effectiveness of various design controllers, the system is tested for protective fault clearing and system start up by using a laboratory synchronous machine matched with a diode rectifier bridge feeding into a dc network set up on the University of Manitoba's real time physical component HVDC simulator. The results are presented in Chapter V.

Further studies are carried out by time domain digital simulation using the EMTDC. It is concluded that the use of diode bridge rectifiers leads to savings in the converter cost. As well, at a remote location an uncontrolled bridge can be mounted in close proximity to the generator. Thus the design of the sending station is simplified. These advantages can be exploited if the system can withstand slow fault clearing and recovery to full power. Our investigations show that approximately 1.5 s is needed for the process.

Chapter II

SYSTEM TRANSFER FUNCTION

The operation of HVDC transmission with diode rectifier requires current control at the inverter . Voltage control is applied at the rectifier only by means of the excitation control of the generator. In order to apply feedback control principle, the transfer function of the system must be determined. The HVDC transmission system shown in Fig.2.1 represents a common HVDC link between an isolated generator and an ac system.

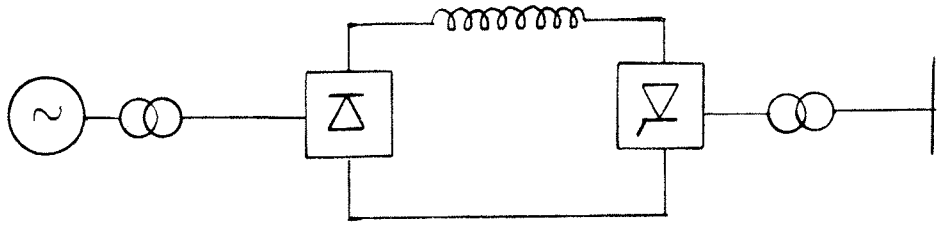

Generator Rectifier Inverter ac system

Figure 2.1: HVDC system

The overall transfer function of the system can be determined by firstly verifying the transfer function of the generator and then that of the dc link. The combination of the

two transfer functions represents the overall open-loop transfer function of the system.

2.1 GENERATOR TRANSFER FUNCTION

The operation of a synchronous generator becomes quite complicated, especially when feeding current into a dc link from a bridge rectifier.

Assume that there is no magnetic saturation in the generator and constant current control is used at the inverter. Under these conditions, in steady state , the generator supplies a constant current to the load while the magnitude of the terminal voltage is controlled by the excitation control. The steady state phasor diagram of the generator is shown in Fig.2.2 [5].

From the diagram shown, let $|Eo/E| = \rho$, the relation between Eo and E can be written

$$\frac{Eo}{E} = \rho e^{j\theta} \qquad (2.1)$$

The dynamic behavior of the generator can be derived from the Park's equations (2.2) to (2.5) [1] and from the phasor diagram shown in Fig.2.3. Park's equations for a synchronous generator are [1] :

$$Ed = p\psi d - Ra.Id - \omega\psi q \qquad (2.2)$$

$$Eq = p\psi q - Ra\ Iq + \omega\psi d \qquad (2.3)$$

$$\psi q = - H(p)\ Lq\ Iq \qquad (2.4)$$

$$\psi d = - F(p)\ Ld\ Id + G(p)\ \frac{Lmd}{Rf}\ Ef \qquad (2.5)$$

H(p),F(p),and G(p) are given by

$$H(p) = \frac{1 + Tq'' p}{1 + Tqo'' p} \qquad (2.6)$$

$$F(p) = \frac{(1+Td' p)(1+Td'' p)}{(1+Tdo' p)(1+Tdo'' p)} \qquad (2.7)$$

and

$$G(p) = \frac{1 + Tkd\ p}{(1+Tdo' p)(1+Tdo'' p)} \qquad (2.8)$$

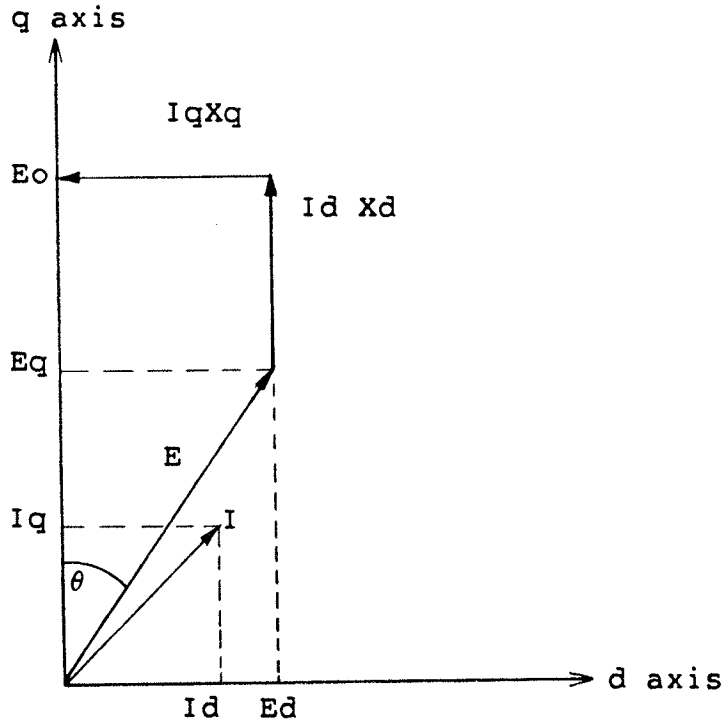

Figure 2.2: Steady state phasor diagram

The various time constants in these expressions are fundamental characteristics of the generator. In steady state, if the armature resistance is neglected, equations (2.2) and (2.3) become

$$Ed = -\omega\psi q \tag{2.9}$$

$$Eq = \omega\psi d \tag{2.10}$$

2.1.1 Small signal variation

Small variation of voltages and flux linkages can be obtained by taking the first derivative of equations (2.4), (2.5),(2.9) and (2.10). Manipulations of the first derivatives and the relations shown in the phasor diagram of Fig.2.3, give the small signal variations of the generator.

Direct axis voltage

The first derivatives of equation (2.9) and (2.4) yield

$$\delta Ed = -\omega\delta\psi q - \psi q\delta\omega \tag{2.11}$$

and $$\delta\psi q = -H(p)\, Lq\, \delta Iq \tag{2.12}$$

hence $$\delta Ed = H(p)\omega Lq\, \delta Iq - \psi q\, \delta\omega \tag{2.13}$$

Define a relative change of quantities Ed, Eq, etc. as

$$\Delta Ed = \frac{\delta Ed}{Ed} \quad ; \quad \Delta Eq = \frac{\delta Eq}{Eq} \quad .....$$

then $$\Delta Ed = H(p)\, \frac{Xq}{Ed}\, Iq\, \frac{\delta Iq}{Iq} - \frac{\psi q\omega\delta\omega}{Ed\ \omega}$$

$$= H(p)\Delta Iq + \Delta\omega \tag{2.14}$$

Quadrature axis voltage

Similarly, the first derivatives of the equations (2.10) and (2.5) yield

$$\delta Eq = \omega \delta\psi d + \psi d \, \delta\omega \tag{2.15}$$

$$\delta\psi d = - F(p) \, Ld \, \delta Id + G(p) \frac{Lmd}{Rf} \delta Ef \tag{2.16}$$

$$\delta Eq = - F(p) \, Xd \, \delta Id + G(p) \frac{Xmd}{Rf} \delta Ef + \psi d \, \delta\omega \tag{2.17}$$

From the phasor diagram shown in Fig.2.2 ,

$$Eq = Eo - Id \, Xd = E \cos\theta$$

$$\frac{\delta Eq}{Eq} = - F(p) \frac{Xd \, Id}{E \cos\theta} \frac{\delta Id}{Id} + G(p) \frac{Xmd \, Ef}{Ecos\theta Rf} \frac{\delta Ef}{Ef} + \frac{\omega\psi d}{Eq} \frac{\delta\omega}{\omega}$$

$$\text{or } \Delta Eq = - \left(\frac{Eo - Ecos\theta}{Ecos\theta}\right) F(p)\Delta Id + G(p) \frac{Xmd}{Ecos\theta} If\Delta Ef + \delta\omega$$

$$\text{or } \Delta Eq = \left(\frac{cos\theta - \rho}{cos\theta}\right) F(p)\Delta Id + \frac{\rho}{cos\theta} G(p)\Delta Ef + \Delta\omega \tag{2.18}$$

2.1.2 Internal commutation voltage

The internal commutation voltage must be introduced as the generator is subjected to the commutation phenomena of the bridge rectifier. The terminals of the generator are short circuited during the commutation period, but the internal commutation voltage of the generator is not zero. This voltage is simply the voltage behind the subtransient

reactance of the machine. The ideal no-load dc voltage of the rectifier is proportional to this voltage. It is therefore necessary to calculate the components of this voltage as a function of the components of current Id and Iq. The diagram shown in Fig.2.3 illustrates this voltage and its components by assuming that the subtransient reactance of the direct axis and that of the quadrature axis are approximately the same.

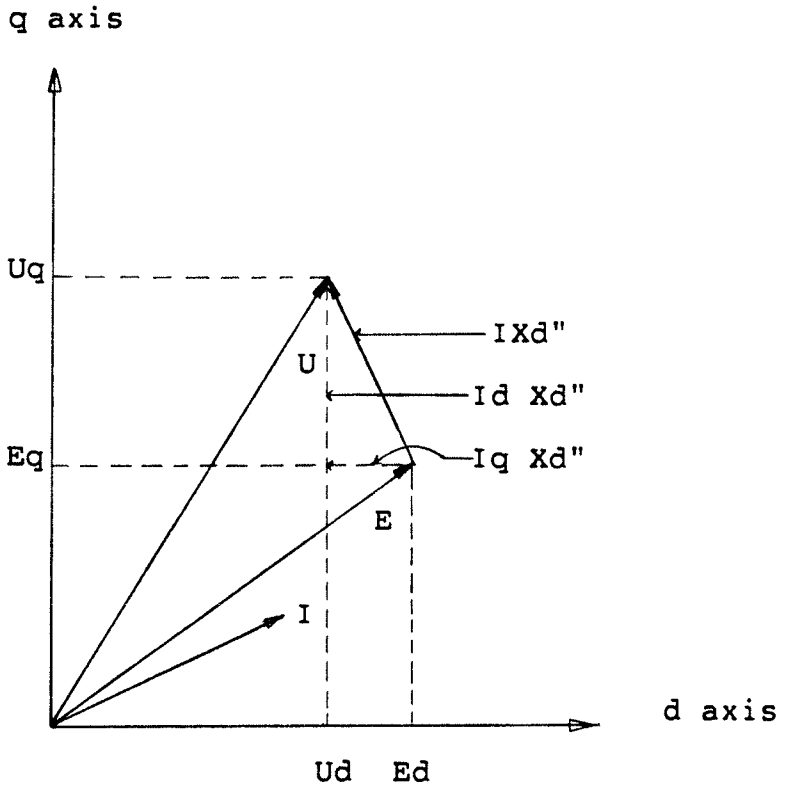

Figure 2.3: Internal commutation voltage

Direct axis voltage variation

The following expressions can be written from the phasor diagram of Fig.2.3 .

$$Ud = Ed - Xd" Iq \qquad (2.19)$$

and

$$Uq = Eq + Xd" Id \qquad (2.20)$$

Define $\left|\frac{Eo}{U}\right| = \rho'$, i.e. $\frac{Eo}{U} = \rho' e^{j\theta'}$

The first derivatives of (2.19) and the relations of equations (2.11) and (2.13) yield

$$\delta Ud = \delta Ed - Xd" \delta Iq - Ld"Iq \ \delta\omega$$

$$= H(p)\omega Lq \ \delta Iq - \psi q \ \delta\omega - Xd" \delta Iq - Ld"Iq \ \delta\omega$$

since $Ud = U \sin\theta'$, then

$$\Delta Ud = -\left(\frac{-H(p)XqIq + Xd"Iq}{Ud}\right)\Delta Iq - \left(\frac{\psi q\omega + Xd"Iq}{Ud}\right)\Delta\omega$$

$$= -\left(\frac{-H(p)Ed + Ed - Ud}{Ud}\right)\Delta Iq - \left(\frac{-Ed + Ed - Ud}{Ud}\right)\Delta\omega$$

$$= [1 - \frac{Ed}{Ud}(1-H(p))]\ \Delta Iq + \Delta\omega$$

$$= [1 - \frac{E\sin\theta}{U\sin\theta'}(1-H(p))]\Delta Iq + \Delta\omega$$

$$\Delta Ud = [1 - \frac{\rho'}{\rho}\frac{\sin\theta}{\sin\theta'}(1-H(p))]\Delta Iq + \Delta\omega \qquad (2.21)$$

Quadrature axis voltage variation

Similarly The first derivatives of (2.20),(2.5) and (2.10) give the following results.

$$\delta Uq = \delta Eq + Xd" \ \delta Id + Ld"Id \ \delta\omega$$

$$\delta Eq = \psi d\delta\omega + \omega\delta\psi d$$

$$= -F(p)LdId\delta\omega + G(p)\frac{Lmd}{Rf} Ef\delta\omega - F(p)Xd \ \delta Id + G(p)\frac{Xmd}{Rf} \ \delta Ef$$

$$\delta Uq = [-F(p)Xd+Xd"] \ \delta Id + [G(p)\frac{Xmd}{Rf}] \ \delta Ef$$

$$+ [-F(p)LdId + G(p)\frac{Lmd}{Rf} Ef + Ld"Id] \ \delta\omega$$

$$\Delta Uq = \left(\frac{-F(p)XdId+Xd"Id}{Ucos\theta'}\right)\Delta Id + G(p)Xmd \ \frac{Ef}{Rf} \ \frac{\Delta Ef}{Ucos\theta'}$$

$$+ [-F(p)XdId+G(p)Xmd \ \frac{Ef}{Rf} + Xd"Id]\frac{\Delta\omega}{Ucos\theta'}$$

$$= \left(\frac{-F(p)(Eo-Ecos\theta)+Ucos\theta'-Ecos\theta}{Ucos\theta'}\right)\Delta Id + G(p)\frac{Eo}{Ucos\theta'}\Delta Ef$$

$$+ \left(\frac{Eq + Ucos\theta' - Ecos\theta}{Ucos\theta}\right)\Delta\omega$$

$$\Delta Uq = \left[1 + \frac{\rho'}{\rho}\left(\frac{cos\theta-\rho}{cos\theta'}\right)F(p) - \frac{\rho'}{\rho}\frac{cos\theta}{cos\theta'}\right]\Delta Id + \frac{\rho'}{cos\theta'}G(p)\Delta Ef + \Delta\omega \quad (2.22)$$

2.1.3 Change of coordinates

The preceding relationships were established in Cartesian coordinates in a system of axes linked to the rotor. But some parameter variations do require small variations in angle. Therefore, a new polar coordinate system is introduced in Fig.2.4 . Further relations can now be developed.

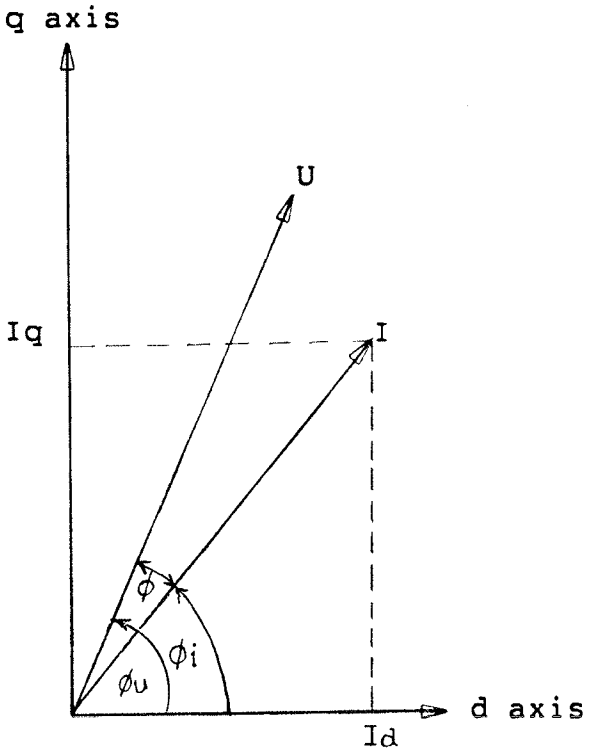

Figure 2.4: Polar coordinates

$$\text{Since} \quad \emptyset u = \emptyset + \emptyset i$$

$$\text{then} \quad d\emptyset u = d\emptyset + d\emptyset i$$

$$Id = I \cos\emptyset i$$

$$\delta Id = - I \sin\emptyset i \, d\emptyset i + \delta I \cos\emptyset i$$

$$\Delta Id = - d\emptyset i \tan\emptyset i + \Delta I$$

$$= - \cot(\theta' + \emptyset)\, d\emptyset i + \Delta I \qquad (2.23)$$

$$Iq = I \sin\emptyset i$$

$$\delta Iq = I \cos\emptyset i\, d\emptyset i + \sin\emptyset i\, \delta I$$

$$\Delta Iq = \cot\emptyset i\, d\emptyset i + \Delta I$$

$$= \tan(\theta' + \emptyset)\, d\emptyset i + \Delta I \qquad (2.24)$$

From equations (2.21) and (2.22), if Udo and Uqo represent the constant speed operation, then the following relations can be written.

$$\Delta Ud = \Delta Udo + \Delta\omega \qquad (2.25)$$

$$\Delta Uq = \Delta Uqo + \Delta\omega \qquad (2.26)$$

where

$$\Delta Udo = \left(1 + \frac{\rho'}{\rho}\frac{\sin\theta}{\sin\theta'}(1 - H(p))\right)\Delta Iq \qquad (2.27)$$

$$\Delta Uqo = 1 + \frac{\rho'}{\rho}\left(\frac{\cos\theta - \rho}{\cos\theta'}\right) F(p) - \frac{\rho'}{\rho}\frac{\cos\theta}{\cos\theta}\Delta Id + \frac{\rho'}{\cos\theta'} G(p)\Delta Ef \qquad (2.28)$$

since $|Uo|^2 = Udo^2 + Uqo^2$

$$2Uo\ \delta Uo = 2Udo\ \delta Udo + 2Uqo\ \delta Uqo$$

$$\Delta Uo = \left(\frac{Udo}{Uo}\right)^2 \Delta Udo + \left(\frac{Uqo}{Uo}\right)^2 \Delta Uqo$$

$$= \sin^2\theta' \Delta Udo + \cos^2\theta' \Delta Uqo \qquad (2.29)$$

and $$\Delta U = \Delta Uo + \Delta\omega \qquad (2.30)$$

since $Udo = Uo \cos\emptyset u$ and $Uqo = Uo \sin \emptyset u$

$$\delta Udo = \delta Uo \cos\emptyset u - Uo \sin\emptyset u\, d\emptyset u \qquad (2.31)$$

$$\delta Uqo = \delta Uo \sin\emptyset u + Uo \cos\emptyset u \, d\emptyset u \qquad (2.32)$$

Manipulation of (2.31) and (2.32) gives the relation

$$d\emptyset u = \sin\emptyset u \cos\emptyset u \Delta Uqo - \sin\emptyset u \cos\emptyset u \Delta Udo \qquad (2.33)$$

The flow graph of these variations are shown in Fig.2.5 .

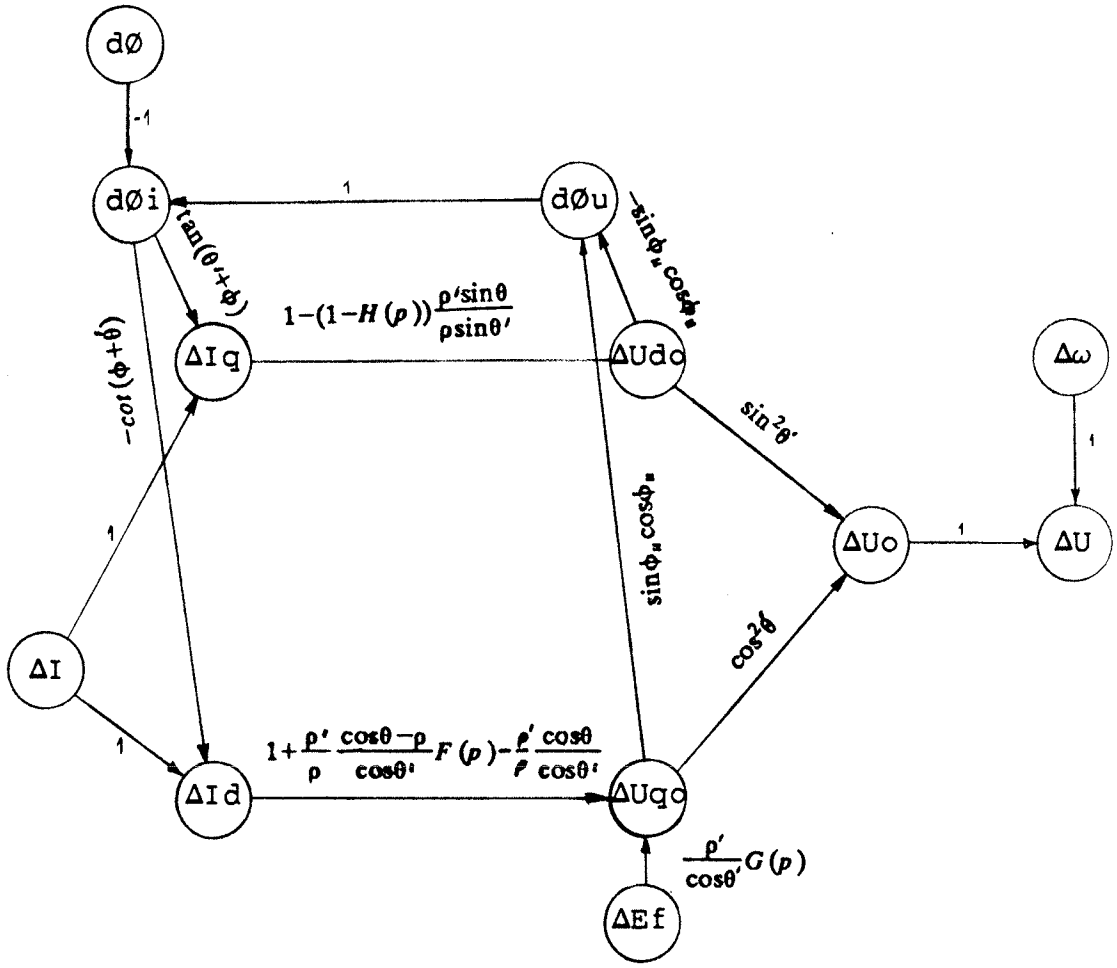

Figure 2.5: Generator flow graph

2.1.4 Approximate generator model

As the operation of the system is assumed to have constant current control at the inverter and constant speed at the generator, the angle Ø ,which depends only on the commutation angle of the diode bridge must be constant. Then, the diagram of Fig.2.5 can be simplified as shown in Fig.2.6 .

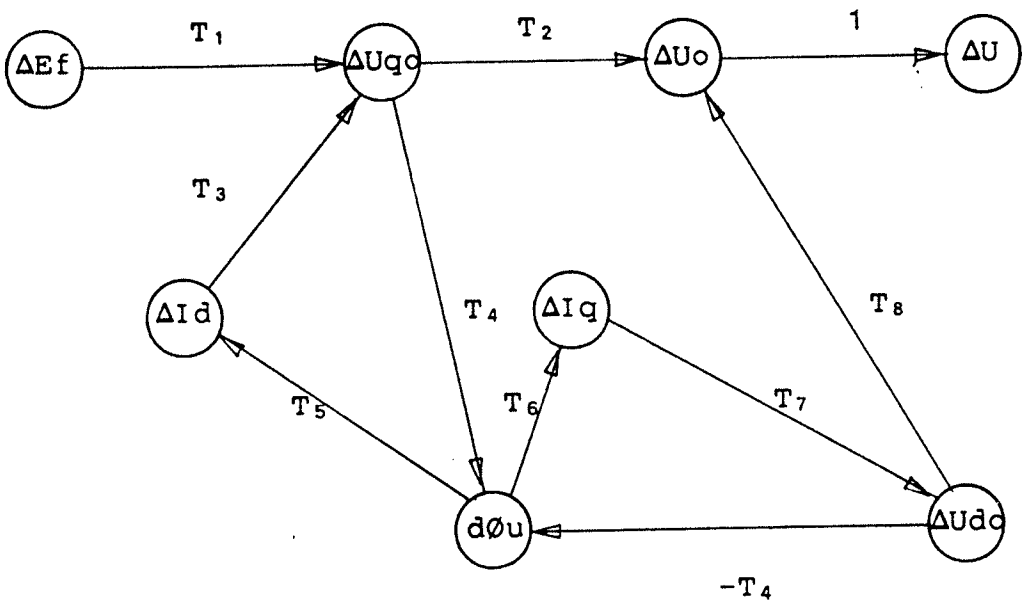

Figure 2.6: Simplified flow graph

where $T_1 = \frac{\rho'}{\cos\theta'} G(p)$

$T_2 = \cos^2\theta'$

$T_3 = 1 + \frac{\rho'}{\rho}\left(\frac{\cos\theta - \rho}{\cos\theta'}\right) F(p) - \frac{\rho'}{\rho}\frac{\cos\theta}{\cos\theta'}$

$$T_4 = \sin\emptyset u \cos\emptyset u$$

$$T_5 = -\cot(\emptyset+\theta')$$

$$T_6 = \tan(\emptyset+\theta')$$

$$T_7 = 1-(1-H(p))\frac{\rho'}{\rho}\frac{\sin\theta}{\sin\theta'}$$

With the application of Mason's theorem [10],[11] , the relation between the quantities ΔU and ΔEf can be found as shown

$$\frac{\Delta U}{\Delta Ef} = \frac{T_1T_2(1+T_4T_6T_7) + T_1T_4T_6T_7T_8}{1 - T_3T_4T_5 + T_4T_6T_7}$$

$$= \frac{T_1T_2 + T_1T_4T_6T_7(T_2+T_8)}{1 - T_4(T_3T_5-T_6T_7)}$$

$$= \frac{T_1(T_2+T_4T_6T_7)}{1-T_4(T_3T_5-T_6T71)} \qquad (2.34)$$

$$= \frac{\frac{\rho'}{\cos\theta'}\left[\cos^2\theta'+\sin\phi_a\cos\phi_a\tan(\theta'+\phi)(1-(1-H(p))\frac{\rho\sin\theta}{\rho\rho\sin\theta'}\right]}{1-\sin\phi_a\cos\phi_a\left[(1+\frac{\rho'}{\rho}\frac{\cos\theta-\rho}{\cos\theta}F(p)-\frac{\rho'\cos\theta}{\rho\cos\theta'})(-\cot(\phi+\theta')-\tan(\phi+\theta)(1-(1-H(p))\right]\left[\frac{\rho\sin\theta}{\rho\sin\theta'}\right]} \qquad (2.35)$$

The terms Tq",Tqo" and Tdo" ,which are included in the expressions (2.6),(2.7)and (2.8), contribute an insignificant response of the system if the frequency response of the system under consideration is not too high. In this case, the frequency response of the system is only in the range of few cycles since oscillatory response of the system is not required. Therefore , the simplified model can be further ap-

proximated if those time constants are neglected. Then equation (2.35) can be reduced to (2.36)

$$\frac{\Delta U}{\Delta Ef} = \frac{\rho'}{\cos\theta'} G(p) \frac{(\cos^2\theta' + \sin\phi_u \cos\phi_u \tan(\phi+\theta'))}{1-\sin\phi_u\cos\phi_u[(1+\frac{\rho'}{\rho}\frac{\cos\theta-\rho}{\cos\theta'}F(p)-\frac{\rho'\cos\theta}{\rho\cos\theta'})(-\cot(\phi+\theta'))-\tan(\phi+\theta')]}$$

$$= Km\ G(p)\ \frac{(1 + Tdo'\ p)}{(1 + Td^*\ p)} \qquad (2.36)$$

where

$$Km = \frac{\rho'}{\cos\theta'} \frac{0.5\sin 2\phi_u \tan(\theta' + \phi) + \cos^2\theta')}{1+0.5\sin 2\phi_u(\cot(\theta'+\phi)(1-\frac{\rho'}{\cos\theta'})+\tan(\theta'+\phi))} \qquad (2.37)$$

and

$$Td^* = \frac{1+0.5\sin 2\phi_u(\cot(\phi+\theta')(1-\frac{\rho'\cos\theta}{\rho\cos\theta'}+\tan(\phi+\theta')T'_{do}+\frac{0.5\sin 2\phi_u}{\tan(\phi+\theta')}(\frac{\rho'}{\rho}\frac{\cos\theta-\rho}{\cos\theta}).Td'}{1+0.5\sin 2\phi_u(\cot(\phi+\theta')(1-\frac{\rho'}{\cos\theta'})+\tan(\phi+\theta'))} \qquad (2.38)$$

The proof of the these is shown in Appendix A. If a more accurate transfer function is required, which takes into account the subtransient time constants, the expression for G(p), which is the multiplier of the equation (2.36) should be written in full. Hence, the more precise transfer function of the generator will be

$$\frac{\Delta U}{\Delta Ef} = Km\ \frac{(1+Tkd\ p)}{(1+Tdo'\ p)(1+Tdo''\ P)}\ \frac{(1+Tdo'\ P)}{(1+Td^*\ P)}$$

$$= Km\ \frac{1 + Tkd\ p}{(1+Tdo'\ p)(1+Td^*\ P)} \qquad (2.39)$$

2.2 DC LINK TRANSFER FUNCTION

The phasor diagram of the generator during the commutation period and the HVDC system under consideration are shown in Fig.2.7 . If all reactances are in per unit values, the dc voltage at the rectifier will be

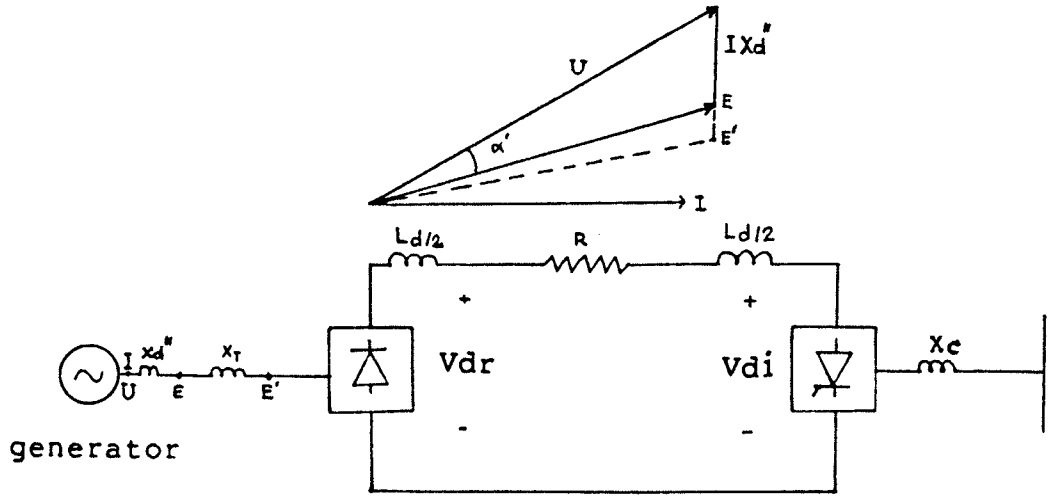

Figure 2.7: dc link diagram

$$Vdr = Vdor\left(1-\frac{Xc}{2}\right)$$

$$= \frac{3\sqrt{6}}{\pi} U \left(1-\frac{Xc}{2}\right) \qquad (2.40)$$

then $$\delta Vdr = \frac{3\sqrt{6}}{\pi} \delta U$$

$$\frac{\delta Vdr}{Vdr} = \left(1-\frac{Xc}{2}\right) \frac{\delta U}{U}$$

$$\Delta Vdr = \left(1-\frac{Xc}{2}\right)\Delta U \qquad (2.41)$$

The dc current flowing in the dc link can be calculated from

$$Idc = \frac{Vdr - Vdi}{R + pL} \tag{2.42}$$

where R = dc line resistance

L = total line inductance

Provided that the inverter has constant-current control, the small variation of terms in equation (2.42) will be

$$\delta Vdr = \delta Vdi$$

$$\Delta Vdr = \frac{Vdi}{Vdr} \Delta Vdi \tag{2.43}$$

Similar to the rectifier, the dc voltage at the inverter is

$$Vdi = Vdoi(\cos\beta + \frac{Xc}{2}) \tag{2.44}$$

The term Vdoi in (2.44) is constant under the assumption that the ac system at the inverter is strong.

Therefore, the small variation of Vdi in equation (2.44) yields

$$\delta Vdi = - Vdo \sin\beta \, d\beta$$

$$\Delta Vdi = - \frac{\sin\beta}{\cos\beta + \frac{Xc}{2}} d\beta \tag{2.45}$$

The signal flow graph for the dc link can then be shown in Fig.2.8 .

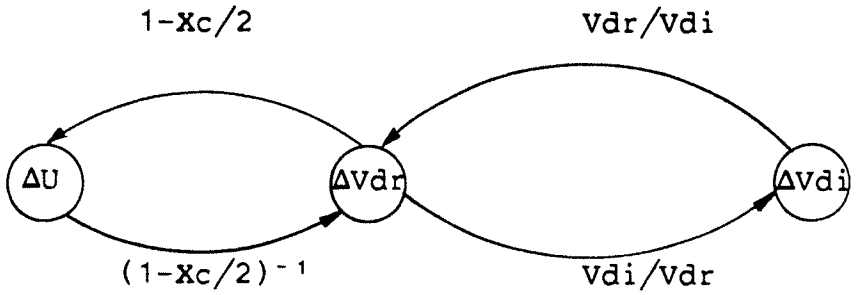

Figure 2.8: dc link signal flow graph

2.3 THE OVERALL TRANSFER FUNCTION

The combination of the generator's transfer function derived in (2.39) and that of the dc link (2.41) results in the overall transfer function of the system. The control parameter of interest for this scheme is the dc voltage at the rectifier, and the input signal to the system is the magnitude of the excitation voltage. Hence, the overall transfer function of the system is

$$\frac{\Delta Vdr}{\Delta Ef} = Km\left(1 - \frac{Xc}{2}\right)\frac{(1 + Tkd\ p)}{(1+Tdo''\ p)(1+Td^*\ p)} \qquad (2.46)$$

2.4 NUMERICAL VALUES

The numerical values of the parameters in the transfer function derived in (2.46) vary with the operating conditions of the generator. For a particular condition, all constants can be calculated from the steady state phasor diagram of the generator. Therefore only the conditions which

are required to connect the machine with the HVDC simulator at the University of Manitoba, are considered.

The HVDC simulator has a scaled back to back dc link. The nominal value of the dc voltage and of the current in the dc link are 50 V and 0.25 A respectively. The system is provided with selectable tap converter transformers for the rectifier and the inverter. Decade capacitors and decade inductors for simulating the harmonic filters are also provided.

2.4.1 Parameter calculation

As the commutation voltage drop, ohmic drop, and the voltage drop across the thyristors have to be included in the calculation of the system, a higher no-load dc voltage is required at the rectifier. It will be shown in Chapter V that for the 6 pulse operation, the ratings of the generator should be

Rated voltage	50 V (line to line)
Rated current	0.18 A

Since the machine constants of the model generator are available at the ratings of 120V, 1/3A [4], then the scaled machine constants in per unit value are

	Xd =	0.605	Xq =	0.580
	Xd' =	0.313	Xq' =	0.537
	Xd" =	0.130	Xq" =	0.110
and	Tdo'=	0.07 s.	Td' =	0.02 s.
	Tdo"=	0.02 s.	Tkd =	0.0022 s.

The approximate value of the power factor on the ac side of the generator when connected to a bridge rectifier can be obtained from the relation

$$\cos \phi = 1 - Xc/2$$

If the commutation reactance is chosen to be 0.15 per unit, the numerical value of the power factor is

$$\cos \phi = 1 - 0.075$$

$$= 0.925$$

$$\phi = 22.33\ ^\circ$$

The steady state phasor diagram of the generator is shown in detail in Fig.2.9.

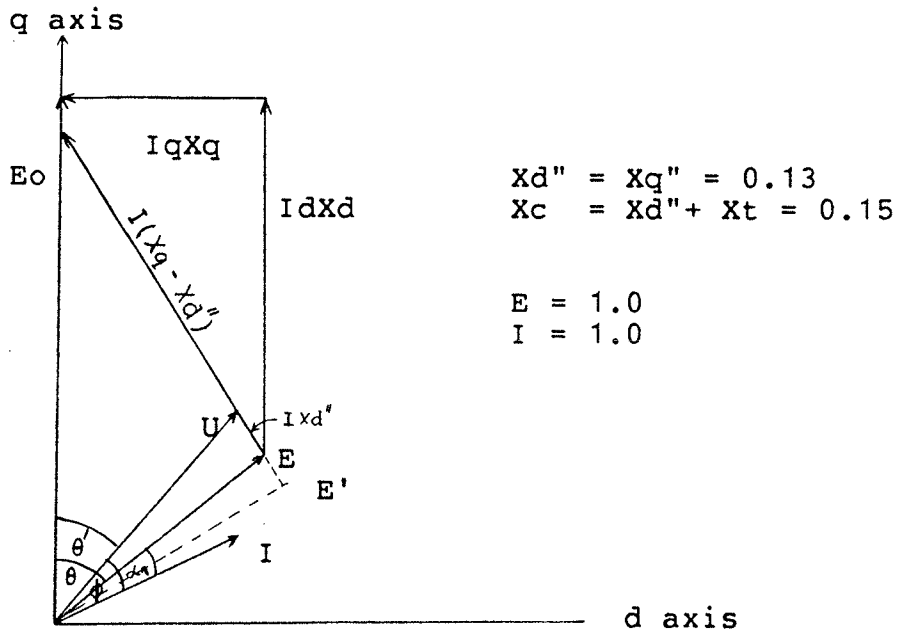

Figure 2.9: Detailed phasor diagram

The magnitude of the commutation voltage U can be calculated from the relation

$$U = IXd''\sin \phi + \sqrt{(IdXd''\sin \phi)^2-(IdXd''^2 - E^2)}$$

$$= 0.13 \sin(22.33) + \sqrt{(0.13\sin(22.33))^2 -(0.13^2 -1)}$$

$$= 1.0421$$

The angle α_1 can be calculated from

$$\alpha_1 = \cos^{-1}(U\cos \phi)$$

From the phasor diagram, the angle θ' can be calculated from

$$\tan \theta' = \frac{I(Xq-Xd'') \cos \phi}{U + I(Xq-Xd'') \sin \phi}$$

$$= \frac{(0.58-0.13) \cos(22.33)}{1+ (0.58-0.13) \sin(22.33)}$$

$$= 0.35547$$

$$\theta' = 19.5688 ^\circ$$

then the electromotive force Eo will be

$$Eo = E \cos\theta' + Id(Xd)$$

$$= E \cos\theta' + \sin(\theta'+\phi)Xd$$

$$= \cos(26.47) + \sin(41.9)*0.605$$

$$= 1.2992$$

then $\rho = Eo/E = 1.2992$ and $\rho' = Eo/U = 1.2466$

and $\phi u = 90 - \theta' = 70.43 ^\circ$

The constants in equations (2.37) and (2.38) can now be evaluated. The calculated values of Km and Td* are

$$Km = 1.3247 \qquad \text{and} \qquad Td^* = 0.0657 \text{ s}$$

Therefore, the overall transfer function of the system under consideration is

$$\frac{\Delta Udr}{\Delta Ef} = 1.3247 \frac{(1 + 0.0022\,p)}{(1+0.02\,p)(1+0.0657\,p)} \qquad (2.47)$$

Chapter III

SYSTEM STABILITY AND COMPENSATION

Implementation of the system with the simulator does require a feedback control signal. In this case it is the dc voltage at the rectifier. Since the controller is very sensitive to the high frequency noise generated by the machine, isolation between the control circuit and the system is necessary. Therefore the dc voltage is fed back into the controller via an isolating voltage transducer. The feedback signal is then compared to the reference voltage giving an error signal to the control system. The block diagram of the excitation control is shown in Fig.3.1 .

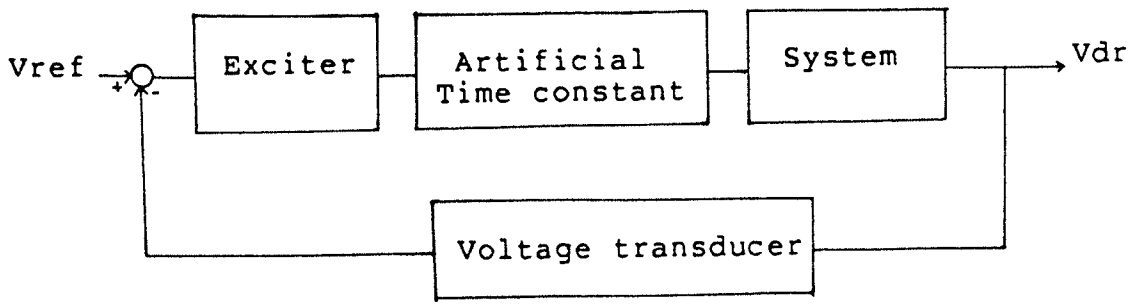

Figure 3.1: Excitation-loop diagram

3.1 ARTIFICIAL TIME CONSTANT

In order to have a realistic system simulation, the field time constant of the machine, which is extremely small, has to be changed. Theoretically, this change can be done by the insertion of a negative resistance into the field circuit of the generator. Practically, this method makes the system very complicated (even for the negative resistance circuit by itself). A moderate solution to this problem is accomplished by the addition of an artificial time constant circuit in the forward path of the system as shown in Fig.3.1. The artificial time constant of the circuit is chosen to be equal to the typical value of the field time constant of waterwheel salient pole synchronous generators, which is about 5 seconds [2].

3.2 EXCITATION-LOOP PARAMETER

The transfer function of each control block of the system in Fig.3.1 is shown in Fig. 3.2 .

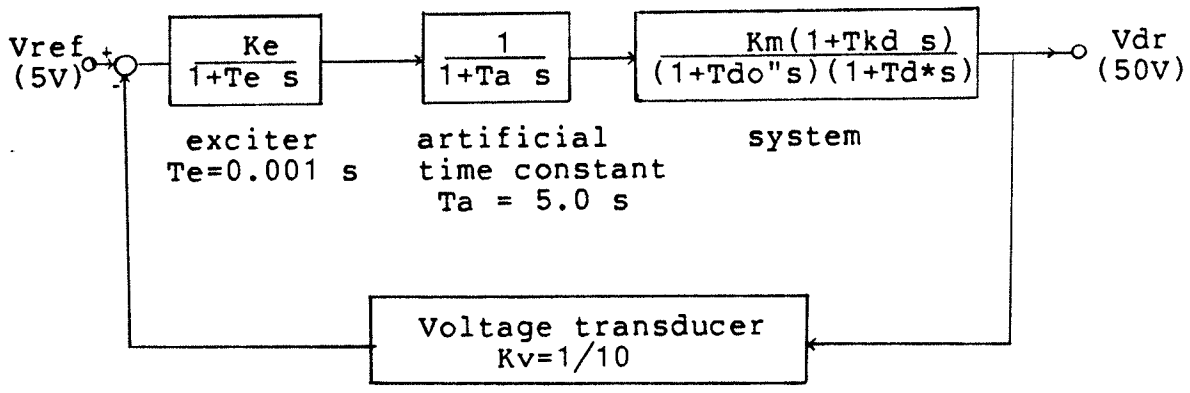

Figure 3.2: Excitation-loop control

As mentioned earlier, the rated dc voltage at the rectifier is 50 V. The dc voltage has to be scaled down before it is fed into the control circuit. Typically, the reference voltage is chosen to be 5 volts then the feedback gain of the voltage transducer should be 0.1 . The voltage transducer is an electronic circuit whose time constant is very small. It also provides electrical isolation between the HVDC system and the control. The exciter available with the generator model is basically an adjustable gain power amplifier. Its time constant is only about 0.001 s, which can be neglected when compared with the larger time constants of the system and the added artificial time constant. The setting of the exciter gain plays an important role in controlling the system.

The system of Fig.3.2 is called type-0 system since there is no integration term in the forward transfer function. The system is stable if the loop gain is not set to a very high value. This type of system control produces a steady state error . The higher the loop gain of the system, the lower the error. If the loop gain is too high the system becomes unstable. The response of the system depends strongly on the setting of this gain. Therefore, an optimal gain has to be known for a particular control system.

3.3 ROOT LOCUS TECHNIQUE

One of the methods for the determination of the optimum gain for a control system is provided by the root locus method. This technique is widely used in system control. Loci of the closed-loop poles are plotted on the s-plane with variation of the loop gain. The performance of the system at any value of the loop gain can be estimated directly from the root locus. In order to apply this technique to this system the characteristic equation of the system has to be specified. The numerical value of the characteristic equation of the system in Fig.3.2 is

$$1 + \frac{KeKmKv(1+0.0022\,s)}{(1+0.02s)(1+0.0657s)(1+5s)} = 0 \qquad (3.1)$$

or

$$1 + \frac{G(1+0.0022s)}{(1+0.02s)(1+0.0657s)(1+5s)} = 0 \qquad (3.2)$$

where G = loop gain $= KeKmKv$ (3.3)

The root locus of the characteristic equation (3.2) is plotted in Fig.3.3. It is found that the system is always stable if the loop gain is less than 360. Normally, the relavant system performance criteria are

1. Rise time
2. Damping ratio
3. Maximum overshoot
4. Settling time
5. Steady state error

These performance measueres can be obtained directly from the root locus plot of the system, if it can be approximated as a second-order system. Consider a system having dominant poles shown in Fig.3.4 . The performance of the system in Fig.3.4 can be evaluated from the location of the system poles as follows [12]:

1. Rise time

$$t_r = (\pi - \beta)/\omega_d \qquad (3.4)$$

2. Damping ratio

$$\zeta = \cos \beta \qquad (3.5)$$

3. Maximum overshoot

$$Mp = e^{-(\frac{\sigma_d}{\omega_d})\pi} \times 100\% \qquad (3.6)$$

4. Settling time

$$t_s = 4/\sigma_d \quad \text{(2\% criterion)} \qquad (3.7)$$

$$= 3/\sigma_d \quad \text{(4\% criterion)} \qquad (3.8)$$

5. Steady state error

$$e_{ss} = \frac{1}{1 + G} \times 100\% \quad \text{(for type-0)} \qquad (3.9)$$

It should be noted here that not all of these specifications necessarily apply to any given case, e.g. there is no need to apply the maximum overshoot criterion to an overdamped system. The steady state error must be kept within a specified range for the system that has this error. In some applications, oscillations of the response can not be tolerated. Thus for a desirable transient response of a second-order system, the damping ratio must lie in the range 0.4 to

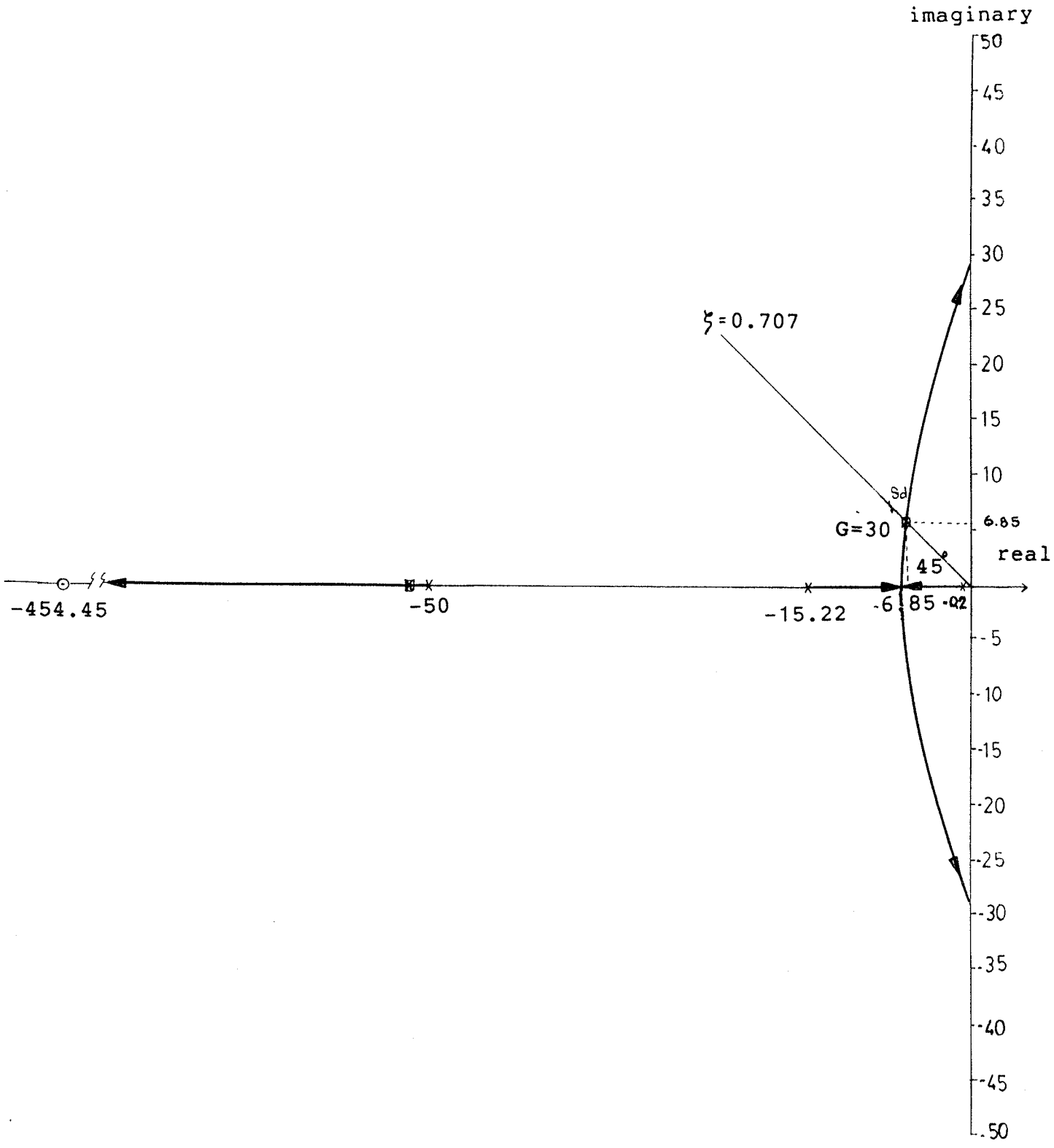

Figure 3.3: Root locus of uncompensated system

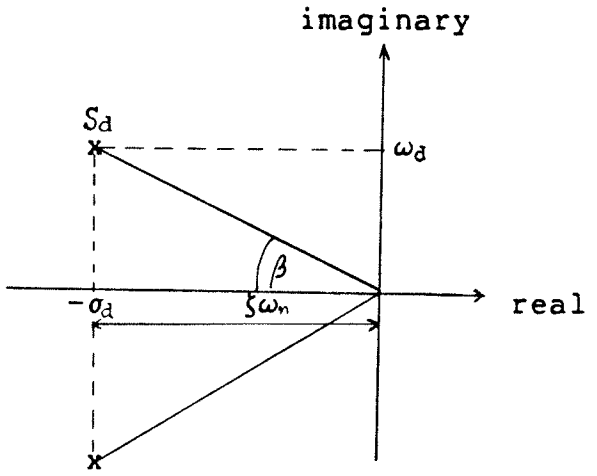

Figure 3.4: Second-order system poles

0.8 . The smaller the value of the damping ratio, the faster will be the rise and the more overshoot will result. If the damping ratio is too large, the system becomes sluggish.

3.4 UNCOMPENSATED SYSTEM

The root locus of the uncompensated system is shown in Fig.3.3 . If the desired damping ratio is chosen to be 0.707, the following performance is obtained from the root locus by using equations (3.4) to (3.9) .

a) Location of dominant poles

$$Sd = -6.85 \pm j\ 6.85$$

b) Closed-loop gain

$$G = 30.0$$

c) Rise time

$$t_r = (\pi-\pi/4)/\omega_d = 0.344 \text{ s.}$$

d) Maximum overshoot

$$Mp = e^{-\pi} \times 100 = 4.32\%$$

e) Settling time

$$t_s = 4/6.85 = 0.584 \text{ s.}$$

f) Steady state error

$$e_{ss} = 100/(1+30) = 3.22\%$$

If the performance of the uncompensated system is examined, it is found that the steady state error as well as the overshoot may be acceptable. However, the system is rather sluggish. In HVDC transmission, the control actions should be made as fast as possible without having excessive overshoot. The rise time of the response will be shorter if higher loop gain or lower damping ratio is selected. Unfortunately , this also results in an increase of the system overshoot, oscillation frequency and the settling time.

Therefore it can be seen that by adjusting only the value of the loop gain, the performance of the system can not be improved as desired. To overcome this problem, the location of the dominant poles should be moved further away to the left in the s-plane. By an addition of a compensation network in the forward path or in parallel with the feedback path of a system, the new root locus can be shaped to the desired location if it is properly designed.

3.5 COMPENSATION TECHNIQUE

Generally speaking, there is no unique method for designing a compensator. A compensation network is designed to satisfy the selected specifications. Practically, most control systems require a trial and error parameter adjustment to get an acceptable performance if it is not possible to satisfy all of the required specifications.

Since the performance of the uncompensated system is quite sluggish, therefore lead compensation, which generally improves the transient response and increases the margin of stability of the system , is required. A lead compensator is a network that provides additional pole and zero into the system. The compensated zero must be placed closer to the $j\omega$ axis in the s-plane as compared to the compensated pole. Normally the pole is placed far away from the zero in order to minimize the effect of the pole on the system response. However, this pole can not ,in practice, be placed too far away from the zero as the system becomes sensitive to high frequency noise. Typically, the position of the pole is limited to be less than 10 times the zero position. But the suitable location of the pole-zero pair is always difficult to find.

3.6 COMPENSATOR DESIGN

Usually, the design specifications are converted into values of damping ratio and natural frequency. By assuming that the compensated system is dominated by two complex poles located nearest to the jω axis ,the location of the compensated pole and compensated zero can be found.

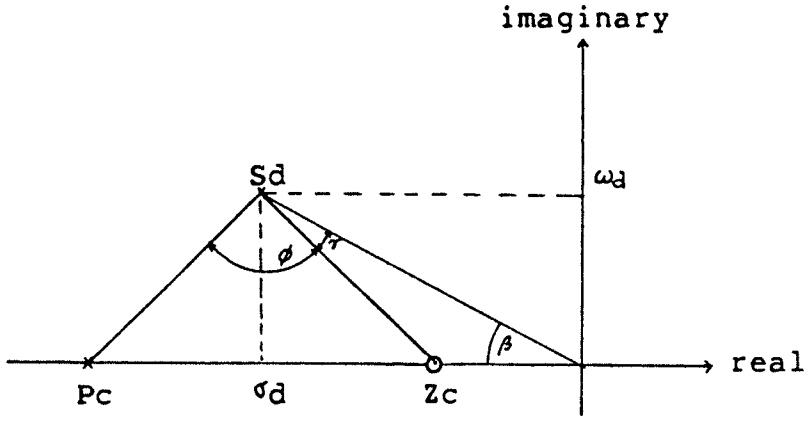

Figure 3.5: Compensated pole-zero location

Consider the s-plane shown in Fig.3.5, if all performance are converted into the desired location of the dominated closed-loop pole Sd ,the suitable position of the compensated pole-zero can be determined by using angle criteria. In the case of a series compensator, if Gc(s) and Gs(s) are the transfer functions of the compensating network and of the uncompensated system respectively, from the angle criterion, it is required that

$$\angle Gc(Sd)Gs(Sd) = \angle Gc(Sd) + \angle Gs(Sd) = \pm 180°$$

$$\angle Gc(Sd) = \emptyset = \pm 180° - \angle Gs(Sd)$$

For the required angle $\emptyset$, there is no unique location of the pole-zero pair. The method of locating the pole-zero position to obtain the largest separation between them is given by drawing a line making an angle γ as shown in Fig.3.5 and having the relation [10],[12]

$$\gamma = 0.5(\pi - \beta - \emptyset)$$

The position of the compensated pole and of the compensated zero on the real axis can be further determined from the diagram. Anyway, the dominant condition is not guaranteed by this method. Therefore, it has to be checked that all other closed-loop poles are either located very close to the open-loop zeros or are relatively far away from the jw axis. In the case that there exists another closed-loop pole in the vicinity of the complex poles, the response will be superimposed by a slow-decaying exponential component. This will result in a longer settling time and the system will be overdamped.

3.6.1 Compensated pole-zero location

It is desired to improve the transient response of the uncompensated system of Fig 3.2 by a lead compensator. If the required specification is to maintain the same damping ratio and reduce the settling time to be less than 0.2 s, the location of the new compensated dominant pole should be at

$$\sigma_d = -4/0.2 = -20$$

$$\omega_d = |\sigma_d| = 20$$

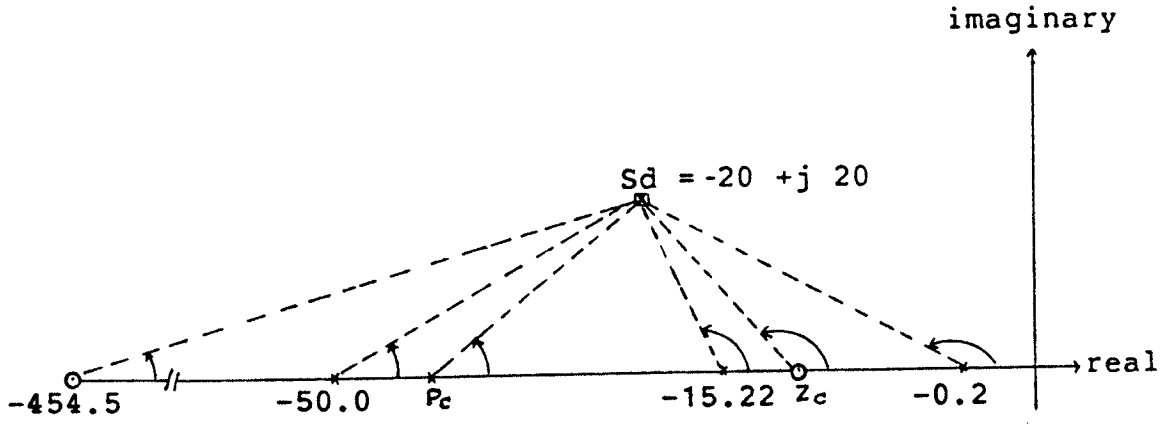

Figure 3.6: Compensated pole-zero

The angle of the uncompensated system at the point Sd is the summation of the angles contributed by the open loop pole-zero of the system. Therefore

$$Gs(Sd) = -269.2°$$

then

$$Gc(Sd) = -180° - (-269.2°) = 89.20°$$

$$\gamma = 0.5(180°-89.2°-45°) = 22.89°$$

The location of the compensated pole and zero found from these values of angle is at

$$Zc = -8.127 \quad Pc = -47.353$$

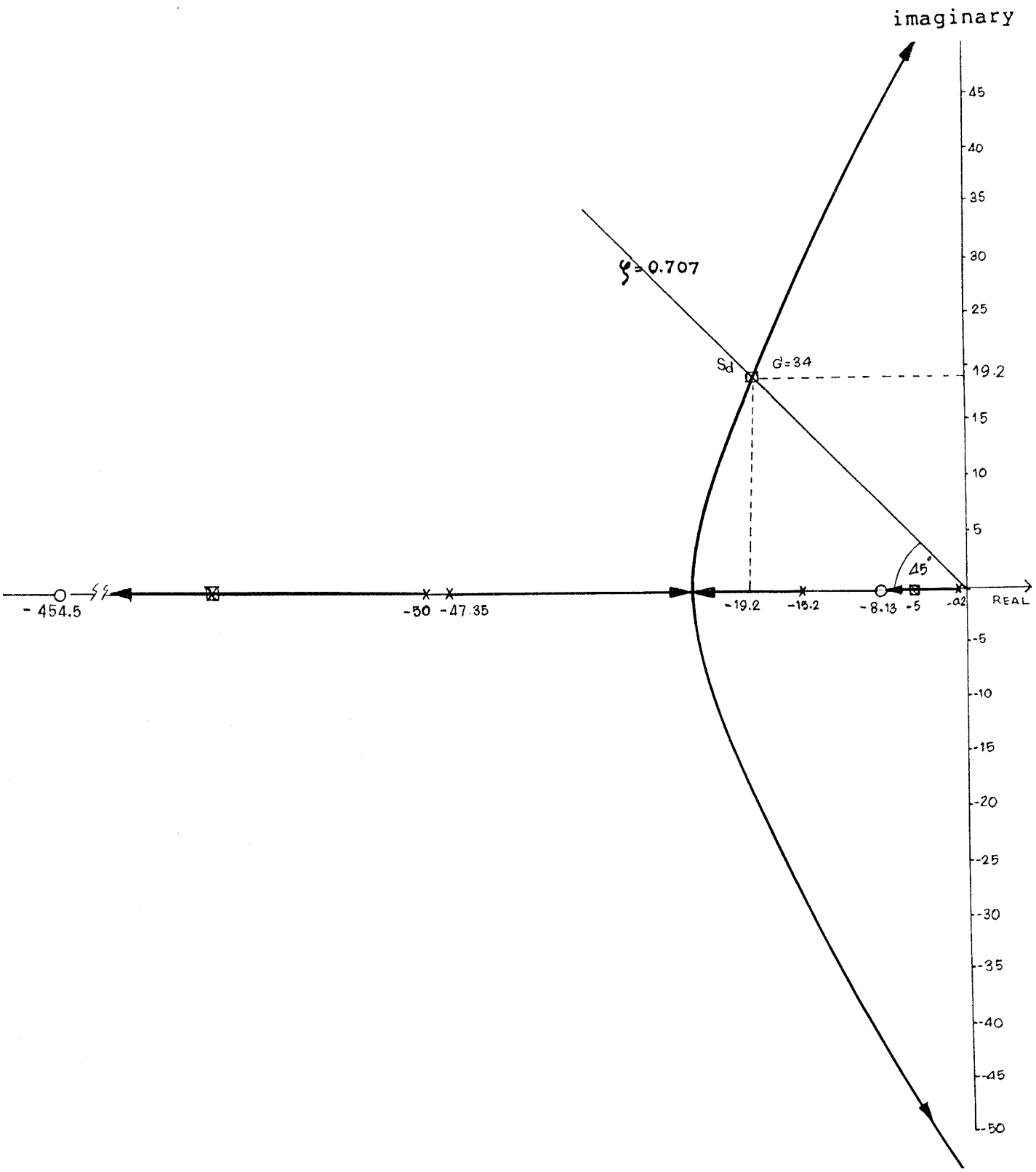

Figure 3.7: Root locus of the compensated system

With these value of the compensated pole-zero pair, the root locus of the compensated system is plotted in Fig 3.7 . It is found that the new locus passes through the points -19.2±j19.2, which are very close to the desired design location. However, the dominant conditions are not held. There is another closed-loop real pole appearing at -5 . The effect of this pole is that the system will be damped to some extent but longer settling time will result.

Practically, if the dominant conditions are to be fulfilled, the compensated zero should be placed to the left of the open-loop pole on the negative real axis in the region where there is no root locus path. If the position of the compensated zero is located at - 17.0 which is to the left of the open-loop pole at - 15.22, the compensated pole is then positioned at -170.0 in order to reduce the effect of this pole on the system. The root locus of this new compensated system is shown in Fig.3.8 . It can be seen that the positions of the dominant poles are very close to those of the old ones but the closed-loop gain is much higher. The time response of the uncompensated system, and that of the compensated system for both techniques are shown in Fig.3.9 . When a comparison of these responses is made the response obtained from the latter technique is preferred.

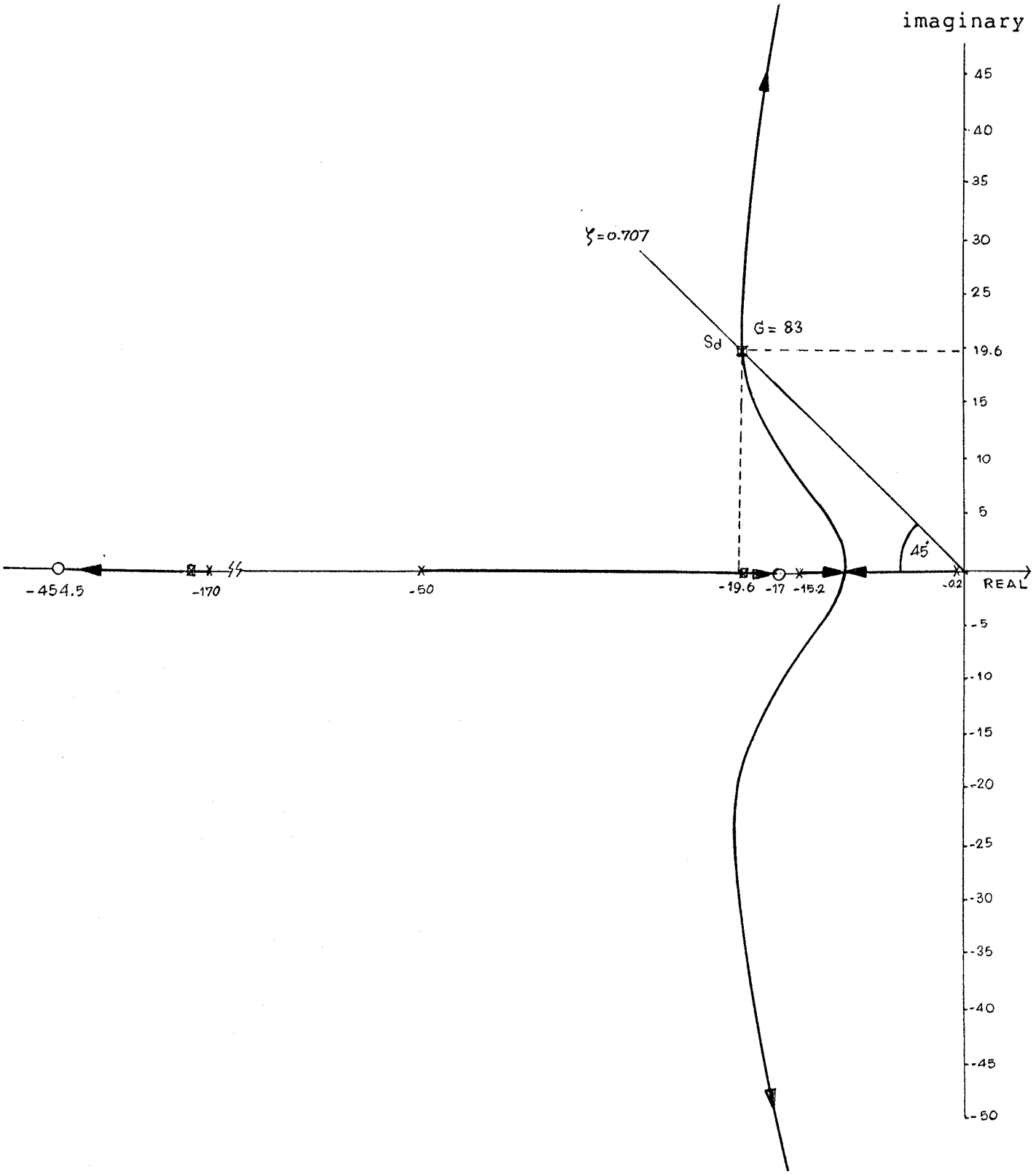

Figure 3.8: Compensated Root Locus of the system

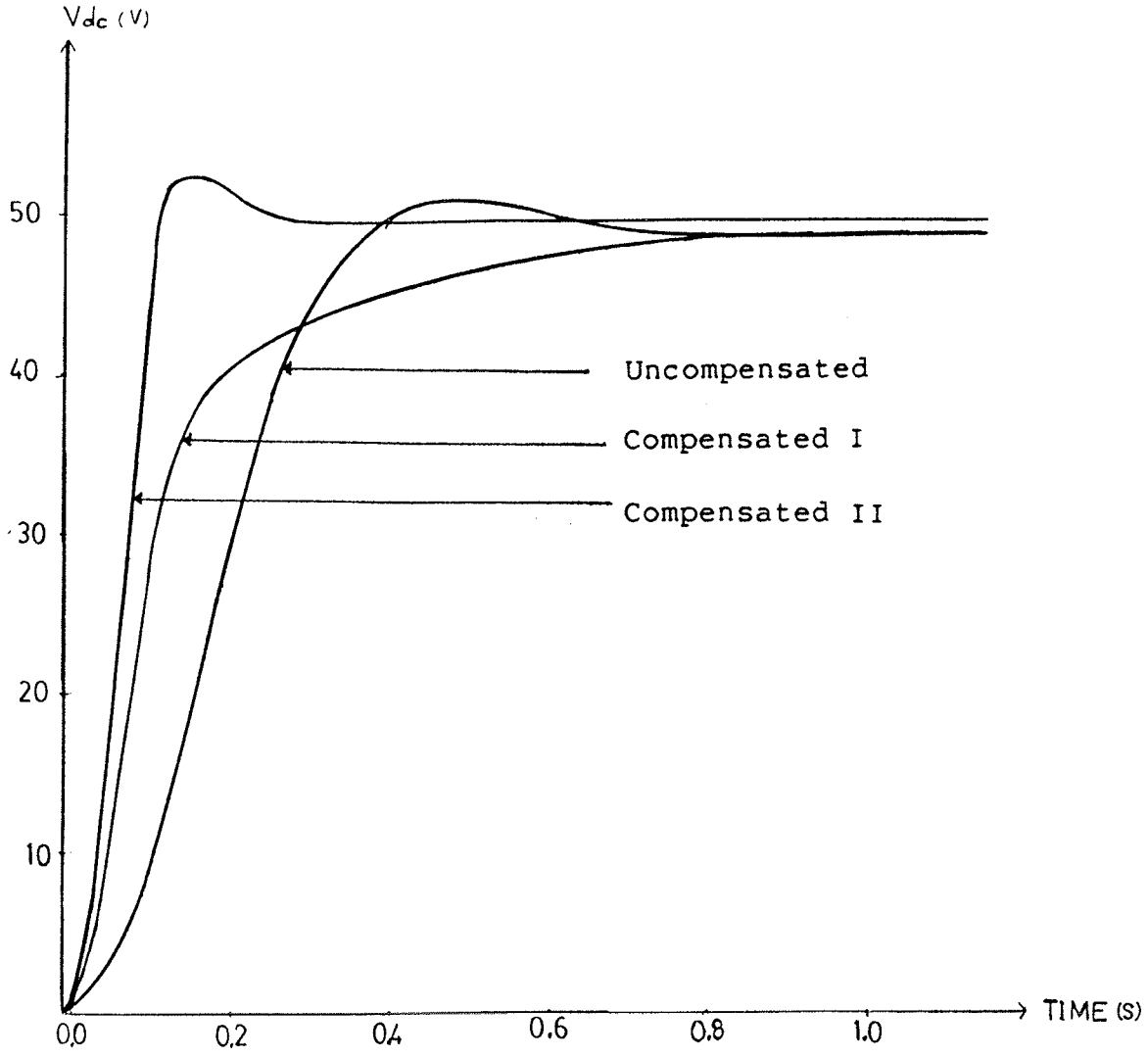

Figure 3.9: Time response of the system

Chapter IV

SYSTEM CONTROLS

An isolated generator with diode bridge rectifier can be connected to a HVDC link in the same way as a thyristor bridge would be. In the absence of the controllability of the diode valves, the control actions will have to to be put on the excitation control of the unit connected generator. The major function of the control is not only to control the dc power flow under normal operation, but also to provide a protective action for the system under fault conditions. In a diode bridge scheme, the dc voltage at the rectifier is continuously controlled by the exciter, thus over-voltage protection is generally not required in the dc link. But it is still essential at the unit connected generator due to its load rejection. Because of the lack of current control at the rectifier, over current protection can be implemented only by the application of dc or ac breakers.

4.1 PROTECTION SCHEMES

Protection schemes for unit connected diode bridge rectifier system are tested by modelling the system on the real time physical component simulator. The protection scheme is characterized by the method of voltage control, overcurrent protection, and the type of system recovery from fault. The

protection schemes shown in Fig.4.1 are tested for their effectiveness. In all cases, the current in the link is detected at the rectifier to determine whether it is greater than its preset value. If the current is greater than the maximum allowable value, e.g. 1.5 p.u. ,the delay circuit will be triggered to produce protective action from overcurrent.

The delay circuit provides controlling signals to : the ac breaker, the excitation control for de-excitation and the inverter for by-passing . To avoid any high induced voltage in the dc link, it is very important to by-pass and block the inverter for some duration after the fault has been detected [6]. This technique allows the current to flow continuously in the dc link in the case that a temporary dc line fault occurs. For the case of a permanent dc line fault, it is not necessary to by-pass the inverter (but blocking is still required) as the current from the rectifier can circulate in the dc link through the fault path. The current has to be reduced to zero by means of ac or dc breakers or by the excitation control of the unit connected generator. Unfortunately, even in the case of a temporary dc line fault, e.g. insulation flashover, the arc can not extinguish itself until the current is reduced to zero. The only way to bring down the current to zero is by using a dc breaker connected in series with the line or an ac breaker in series with the transformer at the rectifier.

The protection scheme shown in Fig.4.1(a) offers the simplest method of system protection against overcurrent. The terminal voltage of the generator is controlled by the automatic voltage regulator in the excitation system. The dc voltage at the rectifier is proportional to the terminal voltage of the generator if the current is held constant. Once overcurrent on the dc side is detected the delay circuit could open the ac breaker for a prescribed period of time to deionize the dc fault. The overcurrent detection could simultaneously issue by-passing control signal to the inverter. To by-pass the inverter, a pair of series connected thyristor bridge arms are forced to conduct while the other thyristor bridge arms are blocked. A short time is required to make sure that the current in the dc line is reduced to zero. Normally, this duration does not exceed 200 ms, which is approximately the time constant of the dc line. After this period of time, the breaker can be reclosed and the system can be restarted. This seems to be the simplest and most effective scheme if the system can be restarted without any excessive overcurrent. Experimentally, it is found that after the breaker has been reclosed the transient overcurrent forces the breaker to open again and again. This hunting may occur many times before the system recovers. Sometimes the system may not recover at all. It can happen because of the inrush of line-charging current when full dc voltage suddenly appears and leads to commutation failure in the inverter. Generally, in conventional HVDC schemes the

inverter can recover by itself from commutation failure. However, when diode rectifier is used, because of the lack of current control at the rectifier commutation failure at the inverter appears as a dc line fault as seen from the rectifier.

To overcome this problem in the restarting process the dc voltage should be increased slowly to avoid inrush overcurrent and commutation failure at the inverter. Protective schemes so modified are shown in Figs. 4.1(b) and 4.1 (c) . Theoretically, there is no difference in voltage control whether the feedback signal is fed from the generator terminal voltage or from the dc line voltage. In practice, the response of the system with dc voltage feedback can be made faster than the ac voltage feedback. This is so because of the time constant of the dc voltage transducer is smaller than that of the ac voltage transducer in which the measured ac voltage is rectified and filtered.

As soon as the overcurrent is detected, the delay circuit provides simultaneously a by-passing signal to the inverter, a signal to open the ac breaker and a signal for reversing the excitation voltage of the generator to collapse the field and therefore the generated voltage. The generated voltage at the terminal of the generator is reduced slowly toward zero because of the large time constant of the field circuit, which is the caused by the artificial time constant circuit previously described. At the same time the dc cur-

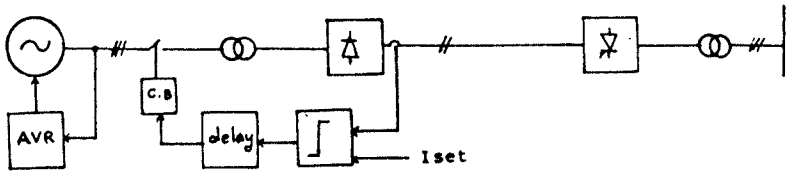

a) ac voltage control with ac breaker

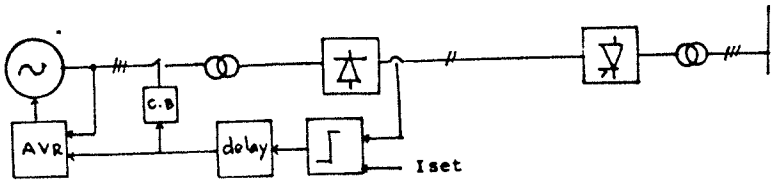

b) ac feedback with field reversed

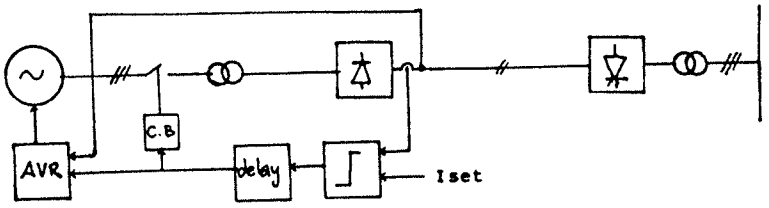

c) dc voltage control with ac breaker

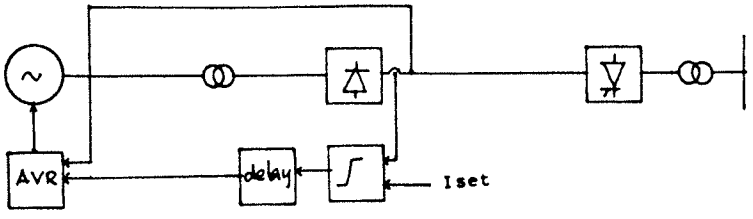

d) dc voltage control without breaker

Figure 4.1: Protection schemes

rent in the link dies down toward zero according to the transmission line time constant. Even though the dc current reaches zero, extra time is required to reduce the terminal voltage of the generator to a low level in order to be able to restart the system without any excessive inrush overcurrent.

The restarting process can begin by first reclosing the ac breaker, deblocking the thyristors in the inverter and then applying the controlled excitation voltage to the generator and current ramp at the inverter. This technique provides a slow rise of both the voltage and the current in the dc link. Since the generator voltage can not be reduced to zero due to its residual magnetism, there is a dc current produced on reclosing the breaker due to line-charging. The peak value of this current is normally less than the threshold of the overcurrent detection circuit, hence, the restart process works satisfactorily.

In the case of a temporary fault that can extinguish by itself, it is not necessary to wait until the generator voltage goes to zero. The ac breaker can be closed at some appropriate voltage level such that the peak inrush current does not exceed the threshold current of the fault detection circuit. This procedure reduces the recovery time after a fault. In practice, the nature of fault is not known in advance, therefore, the current has to be brought to zero by a dc breaker if shorter recovery time from fault is required.

If a dc breaker is used in the line, the ac breaker may be omitted. However, for the protection of the transformer at the rectifier station, an ac breaker may be essential.

The protection system could be much cheaper if no breaker is used as shown in Fig.4.1(d) . This system works only for the case of self-extinguishing temporary dc line faults. The current in the link and in the generator will have a peak magnitude of about 2.5 times its rated value for a short period of time during a fault. The system can be brought into operation when the dc current reaches a certain level. Again, if it is required to reduce the fault current to zero as in the case of a permanent fault, a dc breaker will be necessary. As the voltage control can limit the fault current to a low level, a low interrupting capacity dc breaker can be used.

4.2 CONTROL CIRCUIT

The actual control circuits for all protection schemes described above have many functions in common. The control circuit was therefore designed so that it could be used for testing all protection schemes. The block diagram of the control circuit used for testing the model is shown in Fig.4.2 .

In a real generator, the voltage that can be applied to its field winding is limited to the ceiling voltage of the exciter. The insulation level of the field winding deter-

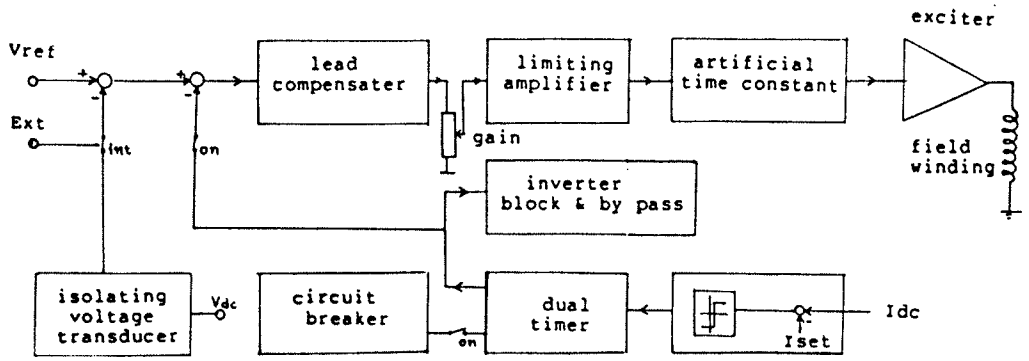

Figure 4.2: Control circuit block diagram

mines the magnitude of the ceiling voltage of the generator. Therefore a limiting amplifier is needed in the control circuit. Typically ,the ceiling voltage of a well designed generator is about ± 5.0 p.u. The higher the ceiling voltage, the faster the field current can be brought to zero. Consequently, the system can recover faster from the dc line fault. The graphs shown in Fig.4.3 illustrate the decay of the field current under different values of reverse ceiling voltages. As can be seen from the graph, the rate of decay of the field current does not only depend on the value of the reverse ceiling voltage, but also on the actual time constant of the field circuit of the generator. The deriva-

tion of the equation governing field current is given in the Appendix B.

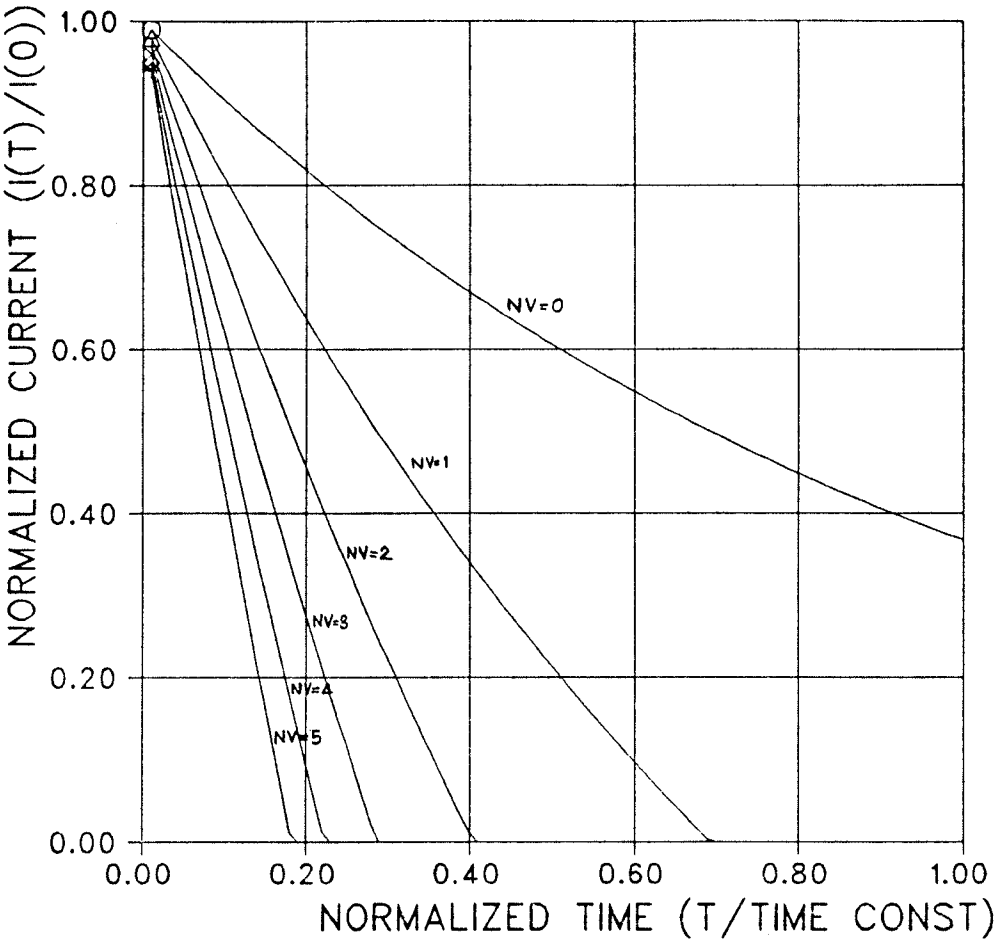

Figure 4.3: **Normalized current decay with reverse voltage**

An alternative method to help increase the decay rate of the field current is to connect a damping resistor in parallel with the field winding when the excitation voltage source is disconnected. The stored energy in the field winding is then rapidly dissipated in the parallel resistor and

the current decays exponentially to zero. The decay rate of the field current as a function of the damping resistance is shown in Fig.4.4 . The derivation of the equation for these relations is also shown in Appendix B.

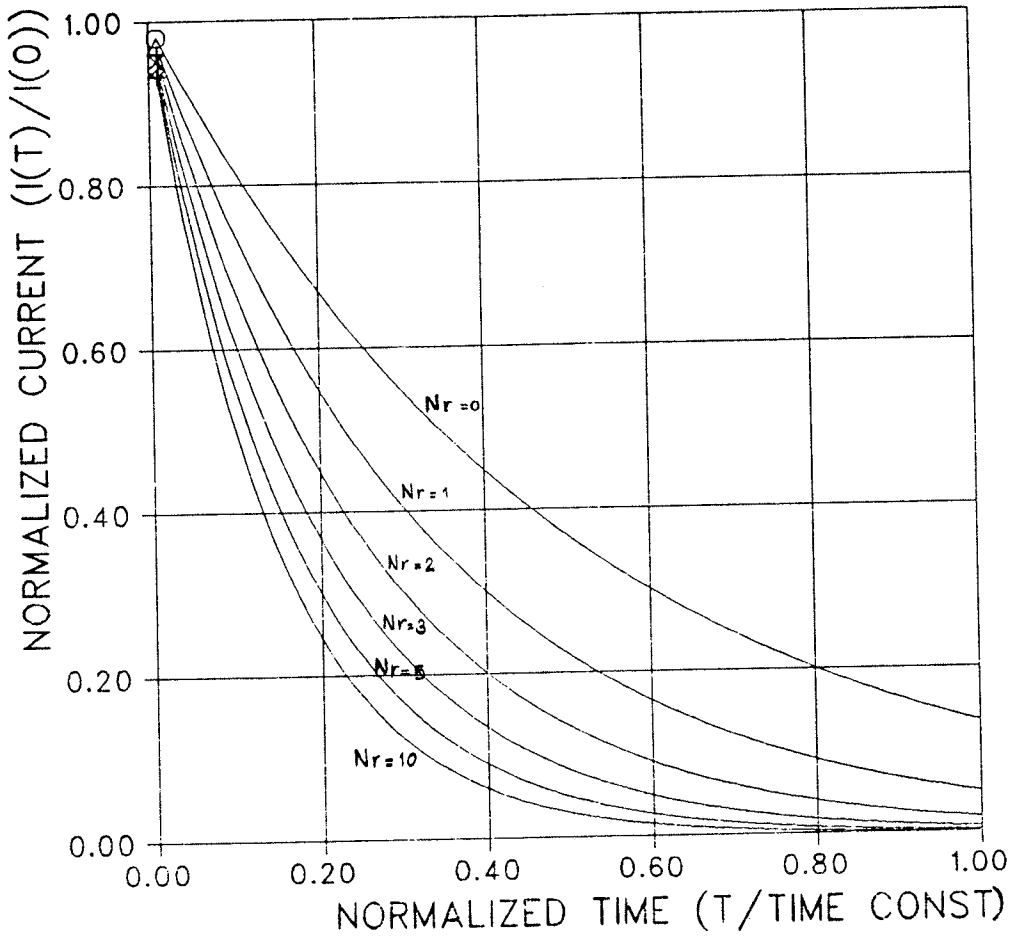

Figure 4.4: Normalized current decay with damped resistor

The value of the damping resistor can however not be made too high else the voltage appearing at the field terminals would be higher than the withstand voltage of the field

winding. Even though this technique is quite simple the current decay rate is not found to be high enough. Therefore, the application of the reversing voltage as the method of de-excitation is recommended.

At the end of the de-excitation period a signal is fed to magnetize the field of the generator and at the same time reclose the ac breaker. Because the ac breaker requires a certain period of time to operate, there is an open circuit in the control loop and system oscillations occur. To solve this problem another signal is required to operate the ac breaker independently. The dual timer circuit is designed to have these properties. The isolating voltage transducer consists of an opto-coupler and a non-linear amplifier which compensates the non-linear characteristics of the opto-coupler. The characteristics of the transducer before and after the application of the non-linear amplifier are shown in Fig.4.5 .

General-purpose operational amplifiers are used in the comparator circuit, amplifiers, artificial time constant circuit and the compensator, in which the location of the compensated pole and zero can be adjusted over a wide range to produce the best response of the system. The design of this circuit is given in Appendix C. The complete control circuit of the scheme is shown in Fig.4.6 . All circuits were mounted on a single board and plugged into the simulator control slot for convenience.

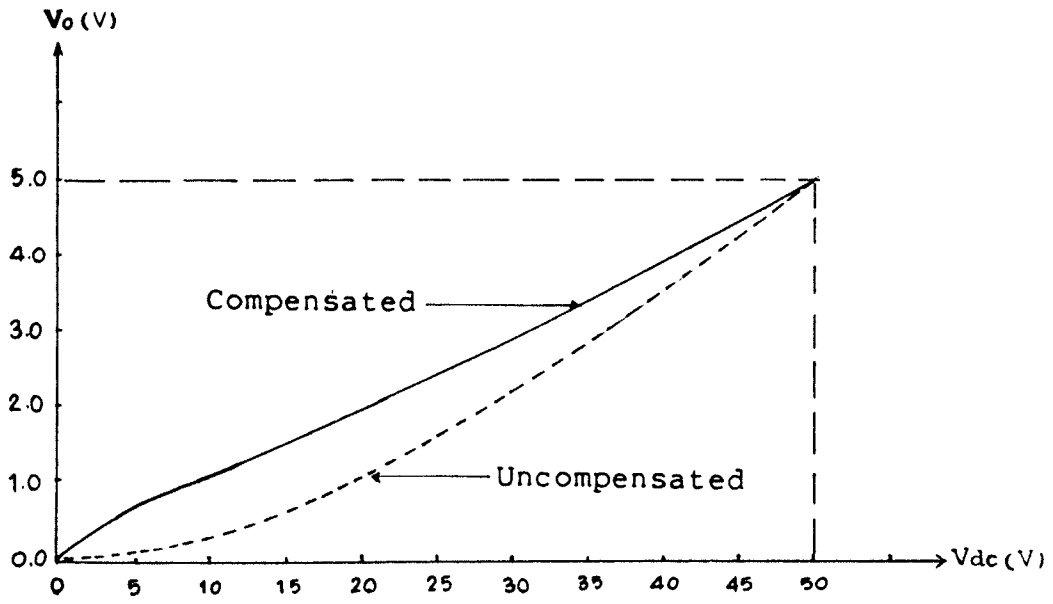

Figure 4.5: Isolating voltage transducer characteristics

As mentioned earlier it is required to ramp the current setting at the inverter in order to achieve a smooth restart after the occurance of a line fault. In real systems, this facility must be available at the inverter. For the simulator studies an additional circuit is required . This circuit is realized by feeding the signal proportional to the original current setting at the inverter and the signal obtained from the time delay circuit into the circuit shown in Fig.4.7 .

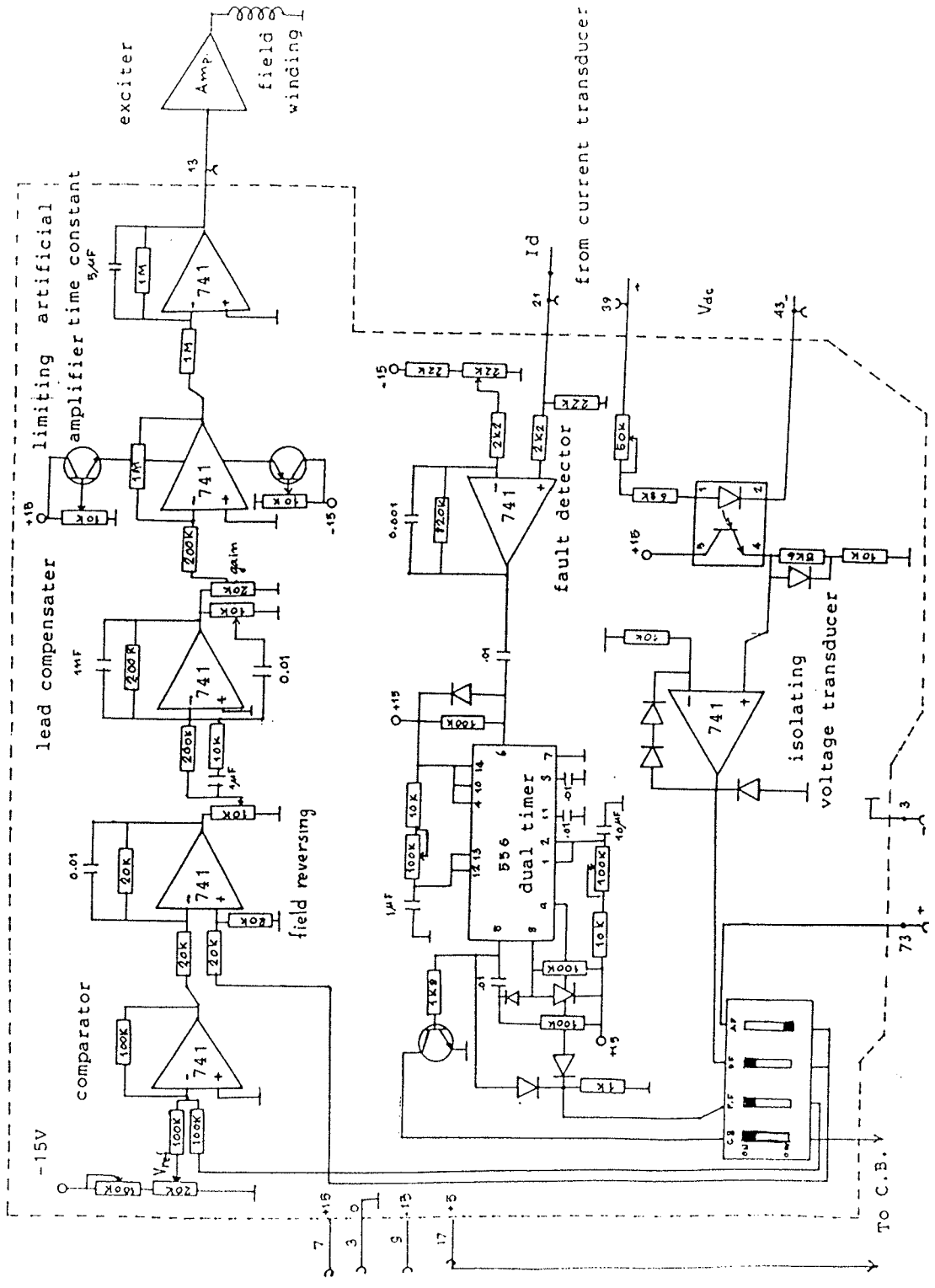

Figure 4.6: Complete control circuit

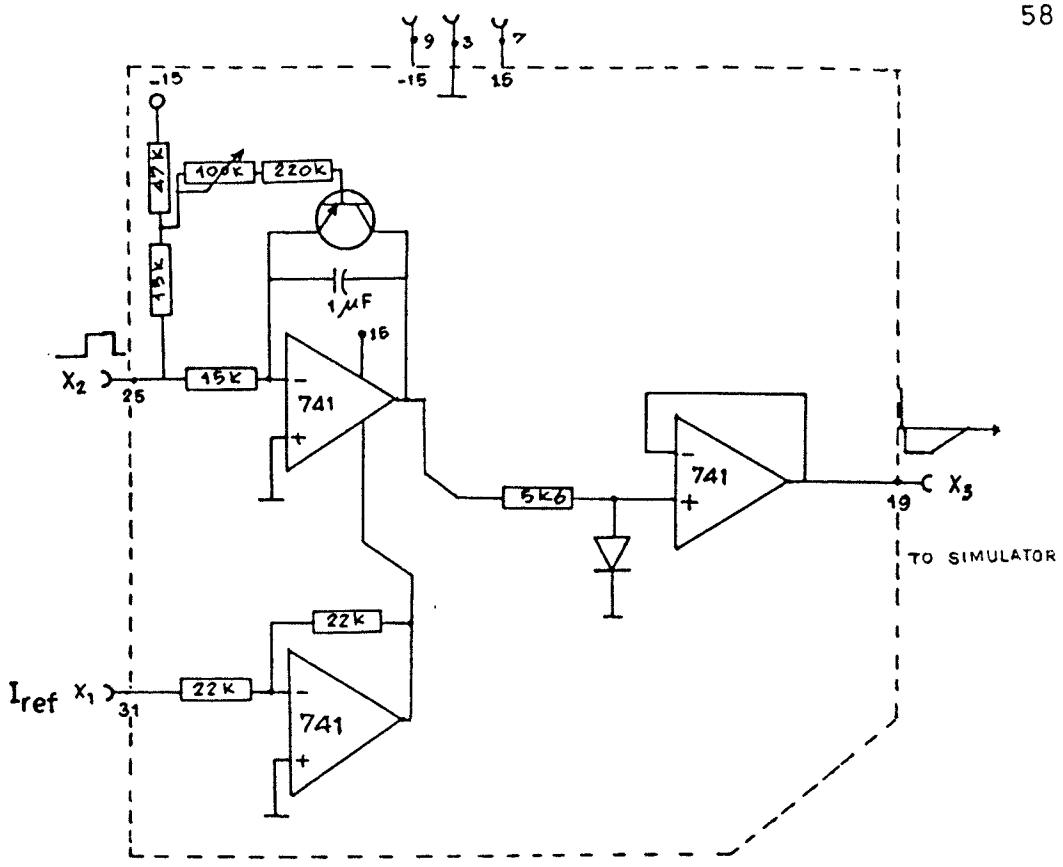

Figure 4.7: Inverter current ramp circuit

The generalized control circuit was used for all protection schemes by selecting a proper combination of dip switches as shown in Fig.4.6 . The controller was tested for all protection schemes. It worked satisfactorily in all cases.

Chapter V

SIMULATOR IMPLEMENTATION AND TEST RESULTS

The performance of a unit connected diode rectifier was studied on the HVDC system simulator. A line fault was simulated by connecting a low resistance from the line to the system ground. The simulator allows a programmable duration of temporary fault on the system. Test results are stored, analyzed and plotted by the computer implanted on the simulator.

5.1 TEST SYSTEM

Scaling calculations have to be performed in order to simulate a given HVDC system on the simulator. The nominal voltage and current levels of the dc link are only 50 V and 0.25 A, respectively . The rated voltage of the converter transformer equipped with a wide range of taps is 100 V (line to line). Thus a wide range of ac voltage can be applied to the primary of the transformer.

5.1.1 Sample system calculations

For a 6-pulse diode bridge operation, the following calculations were made

a) Rectifier terminal

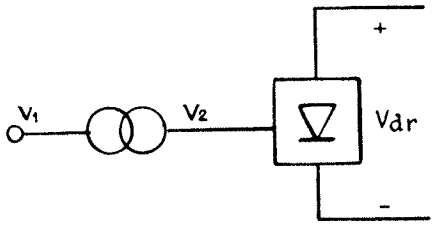

- Secondary voltage:

Assume that the primary and the secondary voltages of the converter transformer are V_1 and V_2 respectively. With the application of a diode bridge rectifier, the dc voltage at the rectifier is given by;

$$Vdr = Vdro(1 - \frac{Xc}{2} - r) - Vth \qquad (5.1)$$

where Vdro = the ideal no-load dc voltage

Xc = commutation reactance (p.u.)

r = internal ohmic drop of the diode (p.u.)

Vth = forward voltage drop of the diode

From the simulator specifications, the following data are available;

Vdr = 50 V

r = 5.6%

Vth = 1.6 V

If the commutation reactance is chosen to be 15% , the no-load dc voltage and the rated secondary voltage can be determined to be :

$$Vdro = \frac{Vdr + Vth}{1 - \frac{Xc}{2} - r}$$

$$= \frac{50 + 1.6}{1-0.075-0.056}$$

$$= 59.38 \text{ volts}$$

The ac voltage at the secondary of the transformer is then

$$V_2 = 59.38/1.35$$

$$= 43.98 \quad V \text{ (line to line)}$$

Practically, it is required to connect the system for both 6-pulse and 12-pulse operation. Therefore, the voltage required for the 12-pulse operation is almost half. Suitable primary voltage of the converter transformer and its turn ratio are chosen to produce 50 Vdc on the dc line.

- Transformer turn ratio :

The turn ratio of the converter transformer at the rectifier defined by the ratio of the valve-side to the ac-side voltages is

$$n_T = V_2 / V_1 = 43.98/50 \qquad (5.2)$$

$$= 0.8796$$

- Primary turns :

The winding diagram of the converter transformer is shown below ;

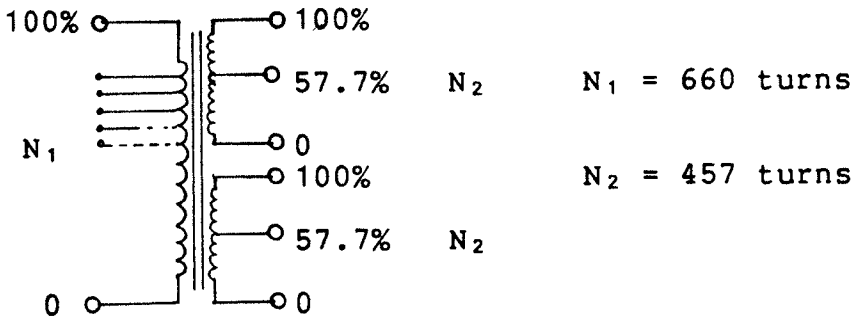

The 57.7% taps at the secondary are provided for the 12-pulse operation. If one of these taps is selected to connect the transformer in Y-Y for a 6-pulse system, the number of primary turns can be calculated from ;

$$n_1 = n_2/n_T$$
$$= (457/\sqrt{3})/0.8796$$
$$= 300 \text{ or } 45.45\%$$

- Transformer base currents :

For 6-pulse operation the secondary and primary base currents are determined from

$$Is = \sqrt{\frac{2}{3}}\, Id = 0.816x0.25 \qquad (5.3)$$
$$= 0.204 \text{ A.}$$
$$Ip = Is\, n_T$$
$$= 0.816x0.25x0.8796$$
$$= 0.18 \text{ amps}$$

- Commutation reactance :

The HVDC system simulator is suited to simulate a back to back scheme. Since the leakage reactance of the transformer is extremely low, an external reactance is added in series with the transformer to represent the leakage reactance of the transformer which is also the commutation reactance of the system. For the HVDC system under investigation, a synchronous generator is directly connected to the primary of the converter transformer. The commutation reactance of the system is the sum of the subtransient reactance of the generator and the leakage reactance of the transformer.

$$Xc = X_T + Xd \qquad (5.4)$$

The leakage reactance of the converter transformer at the base of 50V and 0.18A is measured to be only 1.14% . Since the subtransient reactance of the generator is about 13% , no external reactance is required to satisfy the desired commutation reactance of 15% .

b) Inverter terminal

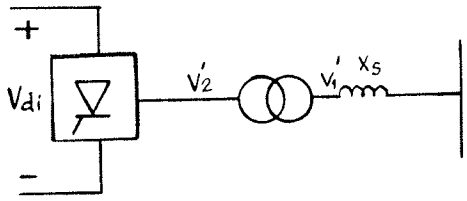

- Secondary voltage :

Equation 5.1 can be applied to the inverter. In this case the nominal value of the firing angle α is about 140 ° [15]. The dc voltage at the inverter is calculated by

$$Vdi = Vdio\ (\cos\alpha - \frac{Xc}{2} - r\ ) - Vth \qquad (5.5)$$

where Vdio is the ideal no-load dc voltage.

If a long transmission line is simulated, the dc line resistance is in the order of 10 ohm, therefore, the voltage drop in the link will be approximately 2.5 V.

$$Vdio = \frac{-47.5+1.6}{\cos 140^\circ - 0.075 - 0.056}$$

$$= 51.168 \text{ V}$$

$$V_2' = Vdio/1.35$$

$$= 51.168/1.35$$

$$= 37.90 \text{ V (line to line)}$$

- Transformer turn ratio :

Since the nominal voltage of the ac system at the inverter (V_1) is 25 V(line to line) [15], then the converter transformer turn ratio is

$$n_T = V_2'/V_1'$$

$$= 37.9 / 25 = 1.516$$

$$n_1 = n_2/n_T$$

$$= (457/\sqrt{3})/1.516$$

$$= 174 \quad \text{or } 26.4\%$$

- Transformer base currents :

The secondary and the primary base currents at the inverter converter transformer are

$$Is = \sqrt{2/3}\ Id = 0.204 \text{ A}$$

$$Ip = Is\ n_T = 1.516 \text{x} 0.204$$

$$= 0.309 \text{ A.}$$

- Commutation reactance :

As previously described, an external reactance is connected in series with the secondary windings of the transformer to represent the leakage reactance of the converter transformer at the inverter.

$$Xc = \frac{0.15 \text{x} (37.9/\sqrt{3})}{0.204}$$

$$= 16.09$$

$$L_C = 42.7 \text{ mH}$$

c) Smoothing reactor :

The smoothing reactor is chosen to have a continuous dc current of at least 10% of the nominal value. Because the set up is 6-pulse no original plant data is available to base on. Experiments show that Ld = 600 mH is a reasonable value [15] .

d) DC filters :

DC filters are connected to the dc line at both rectifier and inverter terminals. The rating of the capacitor depends only on the operating voltage of the dc line and the chosen value of the capacitor. If a 5 μF capacitor is chosen, the rating of the capacitors and the value of the inductors for 6-pulse operation are

$$Pc = C\ Vdc^2 \quad , \omega = 6x377$$
$$= 6x377x5.0\ 10^{-6}x2500$$
$$= 7.06\ Var$$
$$L = 1/\omega^2 C$$
$$= 1/((6x377)^2 5.0\ 10^{-6})$$
$$= 39\ mH$$

e) Harmonic filters :

As less harmonic current is generated at the rectifier harmonic filters are required only at the inverter terminal. The harmonic filters are calculated as follow :

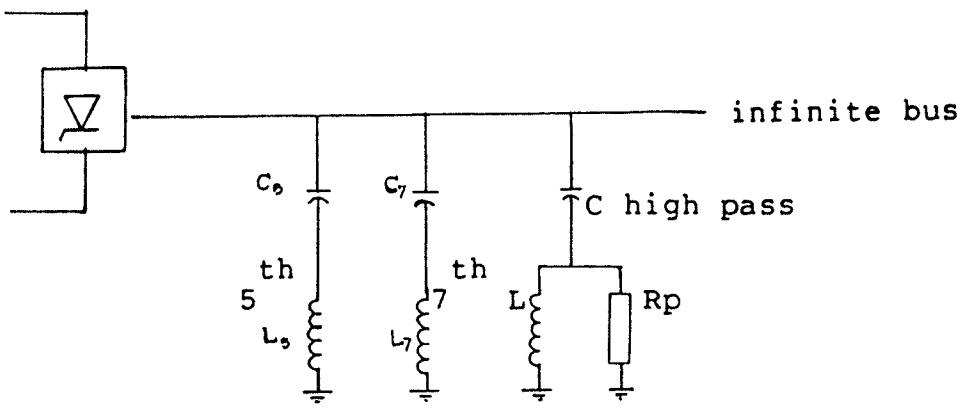

Total VA = 1.05 Vdio Idc

= 1.05x51.16x0.25

= 13.43 VA

real power = VdixIdc

= 47.5x0.25

= 11.875 Watt

reactive power = $\sqrt{13.43^2 - 11.875^2}$

= 6.2729 Var

= 2.09 Var/phase

fundamental current

I_1 = Total VA $/(\sqrt{3}\ V_2)$

= 0.310 A

fundamental voltage

Vph = 25 $/\sqrt{3}$ = 14.43 V

The value of the inductances and the capacitances can be calculated from [14]

$$Pc = Q + \frac{(Vph)^2 (I_1)^2}{h^2 Q} \quad \text{Var} \qquad (5.6)$$

$$C = Pc/[h\omega(Vph)^2] \quad \mu F \qquad (5.7)$$

$$L = 1/(h\omega)^2 C \quad H \qquad (5.8)$$

where h = harmonic order .

The values of the inductances and the capacitances are

5^{th} harmonic , h = 5, ω = 377

$$Pc = 2.09 + \frac{(14.43)^2 (0.310)^2}{25 \quad 2.09}$$

$$= 2.4729 \quad \text{Var}$$

$$C_5 = \frac{2.4729}{5x377x(14.43)^2} = 6.2 \quad \mu F$$

$$L_5 = 1/[(5x377)^2 x 6.2\ 10^{-6}] = 45.5 \quad mH$$

7^{th} harmonic , h = 7 , ω = 377

$$Pc = 2.09 + \frac{(14.43)^2 (0.310)^2}{49x2.09}$$

$$= 2.285 \quad \text{Var}$$

$$C_7 = 2.285/[7x377\ (14.43)^2] = 4.16 \quad \mu F$$

$$L_7 = 1/((7x377)^2 x 4.16\ 10^{-6}) = 39.6 \quad mH$$

High pass filter (12^{th})

$$Pc = 2.09 + \frac{(14.43)^2(0.310)^2}{12x12x2.09}$$

$$= 2.1564 \quad \text{Var}$$

$$C_{12} = \frac{2.1564}{12x377x(14.43)^2}$$

$$= 2.3 \quad \mu F$$

$$L_{12} = 1/[(12x377)^2\ 2.3\ 10^{-6}] = 21.2 \quad \text{mH}$$

for low Q factor, $Q_L \approx 2$

$$Rp = 2x\omega L_{12}$$

$$= 2x12x377x21.2\ 10^{-3}$$

$$= 200\ \Omega$$

f) System impedance

Since the capacity of the dc system is much lower than the capacity of the ac system at the inverter. To simulate a realistic strong ac system at the inverter, a reactance is connected in series with the ac system at the inverter as shown.

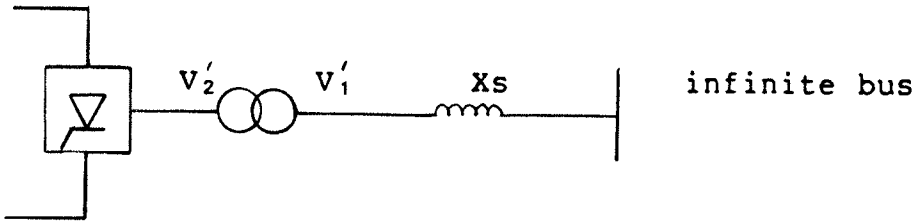

Assume that the short circuit capacity of the ac system at the inverter is 10 times greater than the transmitting power of the dc system, therefore ;

$$SCC = 10\ Vd\ Id$$

$$= 10 \times 47.5 \times 0.25$$

$$= 118.75 \quad VA$$

The value of the simulated system impedance Xs is then calculated from

$$Xs = \frac{(V_1/\sqrt{3})^2}{SCC}$$

$$= \frac{(25/\sqrt{3})^2}{118.75}$$

$$= 1.75 \quad \Omega$$

$$Ls = 4.65 \text{ mH}$$

Similarly the system can be calculated for a 12-pulse operation. The simulated system and the measuring points are shown in Fig.5.1 .

5.2 SYSTEM TESTING

The simulated system was tested experimentally for its performance and the effectiveness of the protection schemes described in Chapter 4. The system set up and the measuring points of interest are shown in Fig.5.1 . The system was started by running the generator at zero excitation while the desired dc current in the link was set at the inverter terminal. The excitation was increased slowly until the max-

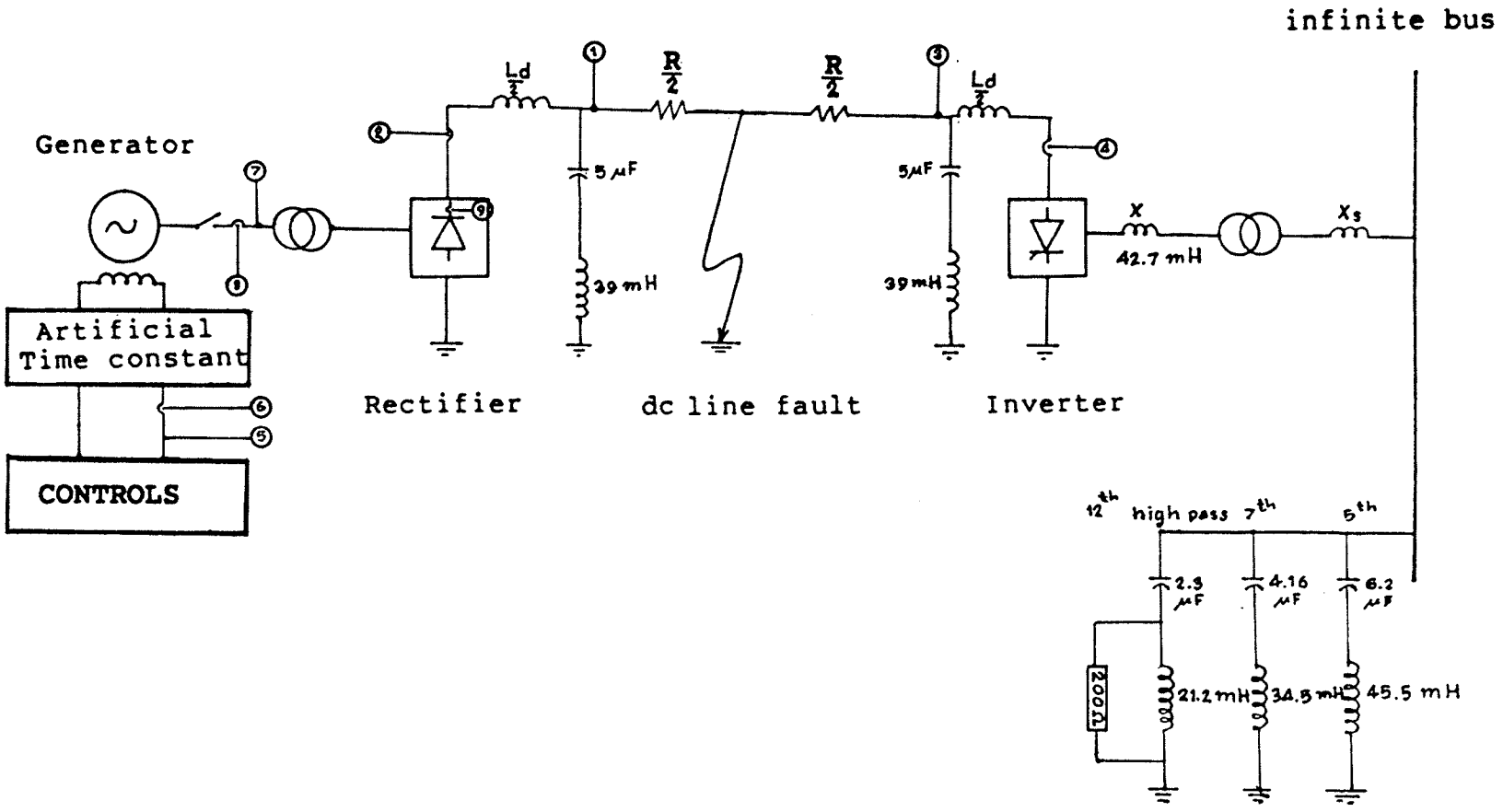

Figure 5.1: Simulated system and measuring points

imum allowable gain of the control was reached. After the system reached its steady state, a temporary line fault was created at the middle of the transmission line to evaluate the protection schemes. The current and voltage waveforms at the measuring points were monitored and recorded by a digital storage oscilloscope. The waveforms were transfered to a mini computer and plotted to examine the behavior of the system in detail.

The dc voltage waveforms at the rectifier (Vdr) and the inverter (Vdi) were measured at points 1 and 3 respectively. These waveforms showed the response of the dc voltages at both ends of the dc link after the fault had occurred. The dc currents at the rectifier (Idr) and at the inverter (Idi) were observed at points 2 and 4 . The current waveform at the rectifier showed the magnitude of fault current and current stresses on the diode bridge. These stresses are to be used for dimensioning of the diode bridge rectifier.

The excitation voltage (Vf) and the excitation current (If) were also monitored at points 5 and 6 to examine the exciter response. At points 7 and 8 the ac voltage (Vac) and ac current (Iac) at the primary of the converter transformer for the rectifier were also displayed. The waveform of the diode current inside the bridge rectifier during the line fault was monitored in detail at point 9 to investigate the severity on the diode rectifier.

5.3 TEST RESULTS

The results were recorded for all protection schemes with different system arrangements. For the 6-pulse operation, the system was also tested without the dc filters to examine whether they could be removed. The response for 6-pulse and 12-pulse operation with dc filters showed a slight difference in the dc voltage waveform. These waveforms are studied in detail in the following section.

5.3.1 AC voltage control with ac breaker

The results of the first protection scheme mentioned in Chapter IV for 6 pulse operation without and with the dc filters are shown in Fig.5.2 and Fig.5.3 respectively. The response of the 12-pulse operation of this scheme are illustrated in Fig.5.4 . At the time before the fault was created all of the waveform amplitudes were marked 1.0 pu . At the instant of the dc line fault, the dc current at the rectifier increased sharply. The fault detection circuit was triggered when the dc current at the rectifier was greater than 1.5 pu . As the breaker could not be opened simultaneously, the peak dc current at the rectifier had reached about 2.5 p.u. when the breaker was opened. As soon as the breaker opened, the generated voltage at the terminal of the generator rose owing to the load rejection of the generator. The excitation voltage as well as the excitation current were reduced to keep the terminal voltage constant. Since only a temporary line fault was studied, the duration of the fault

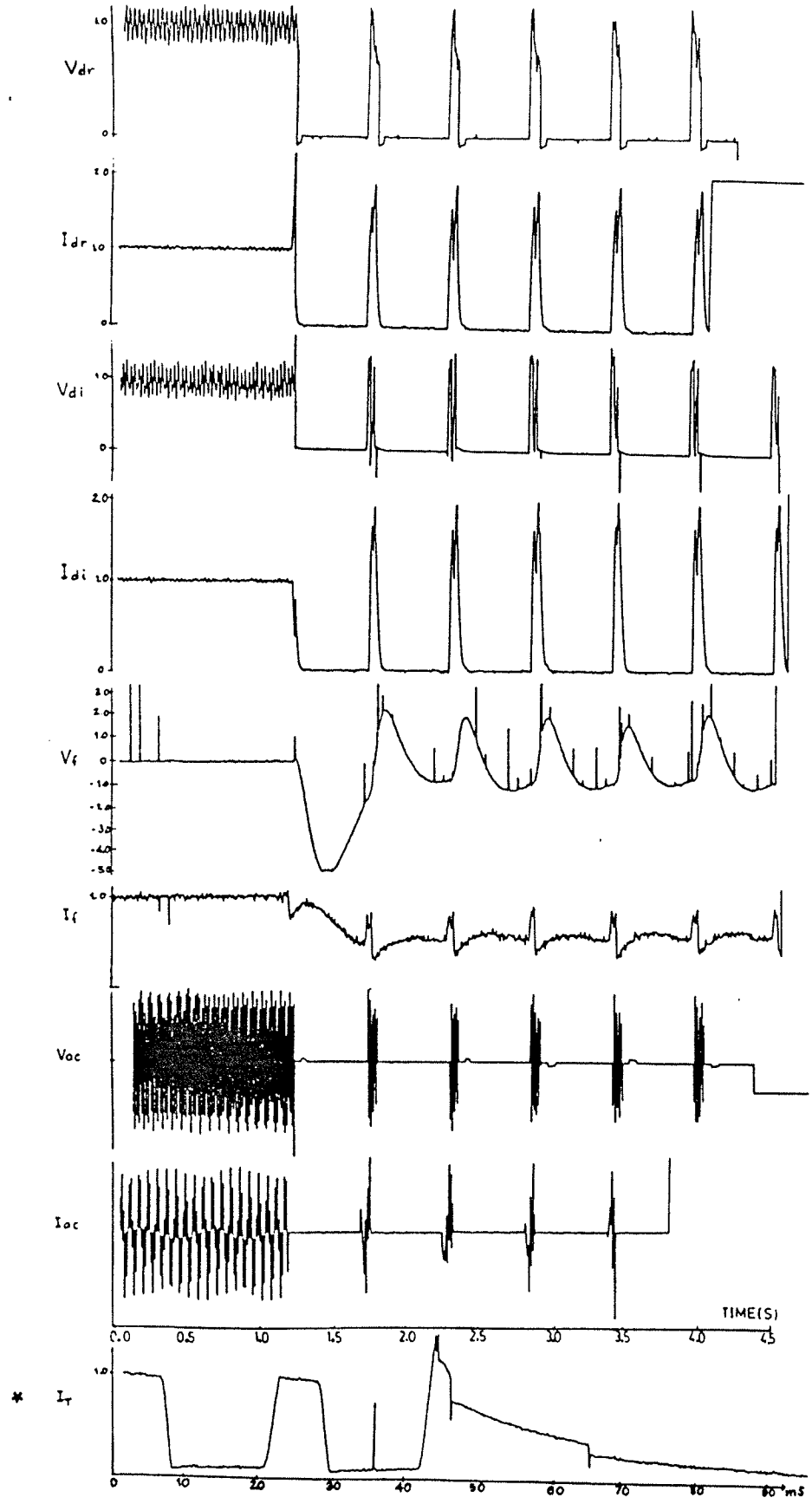

Figure 5.2: Response of scheme (a) for 6 pulse without dc filter

* one bridge arm current with enlarged time scale

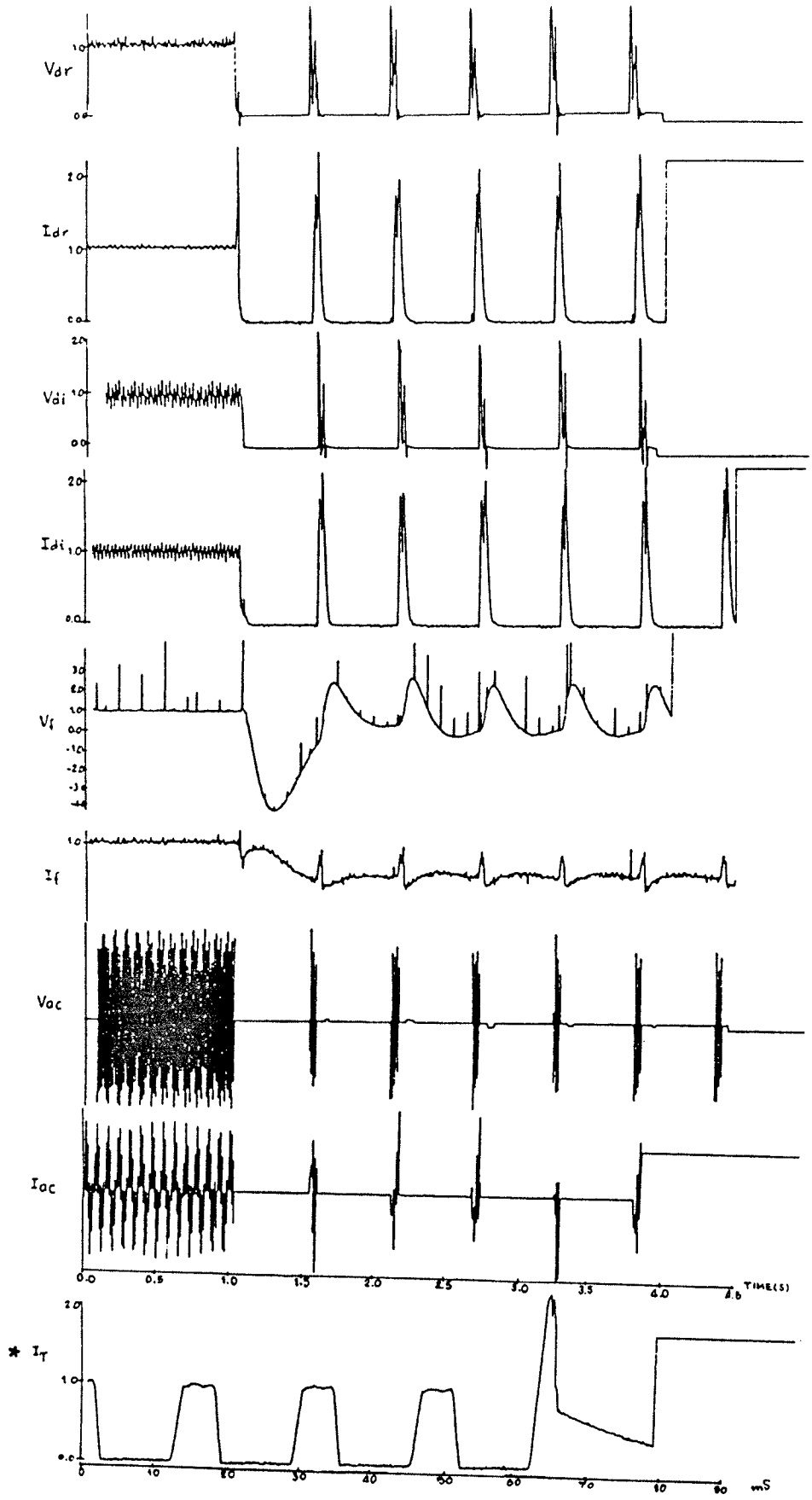

Figure 5.3: Response of scheme (a) for 6 pulse with dc filter

* one bridge arm current with enlarged time scale

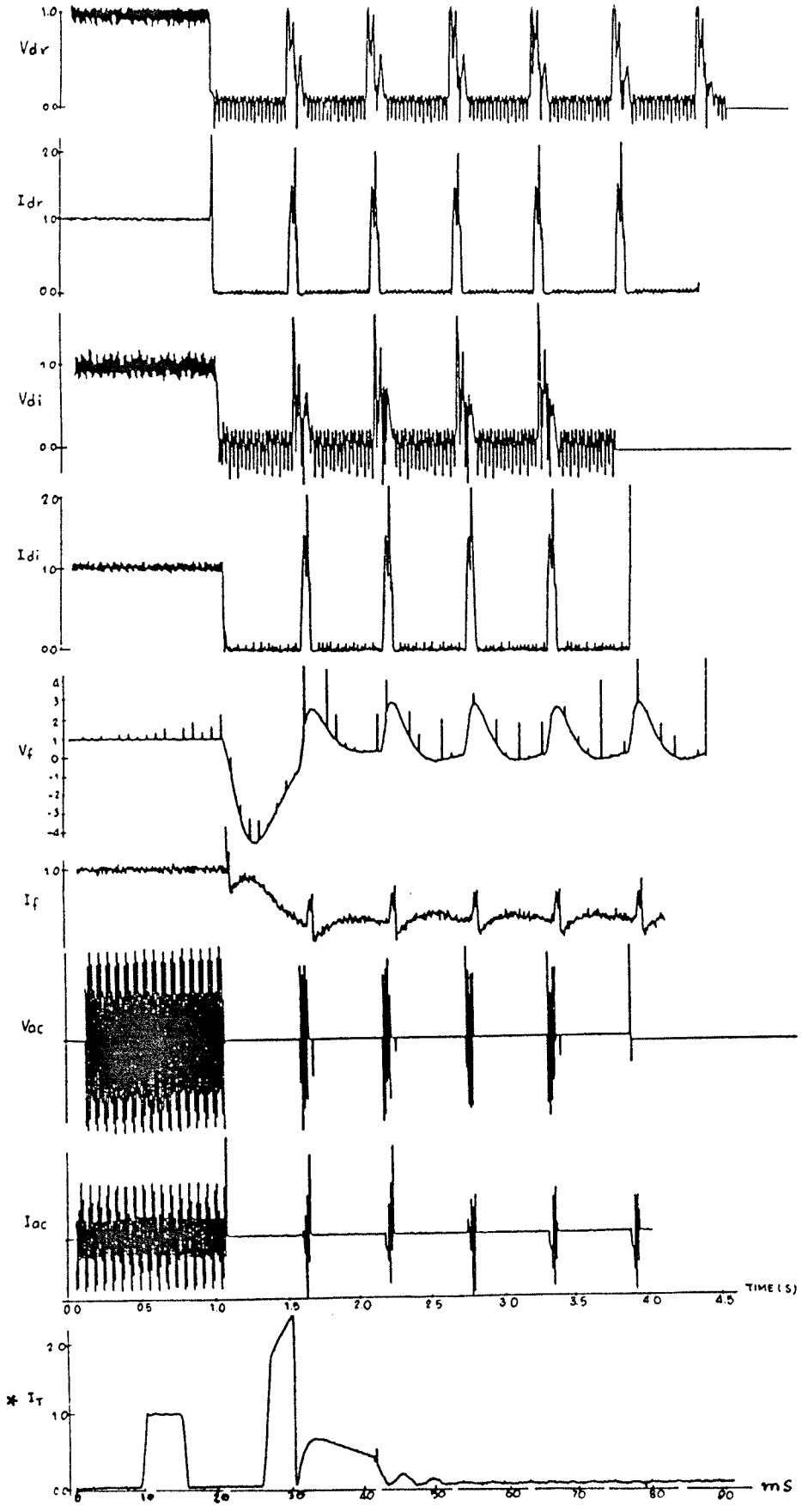

Figure 5.4: Response of scheme (a) for 12 pulse with dc filter

* one bridge arm current with enlarged time scale

was set to 100 ms. After this interval, the dc current continued to flow in the dc link through the by-passed bridge arms at the inverter, which were by-passed as soon as the line fault was detected at the rectifier. The dc currents reached zero within 0.2 s for all system arrangements. The breaker was reclosed 0.5 s later by the control signal from the time delay circuit.

At the time of reclosing the ac breaker the dc currents and the dc voltages in the link increased rapidly. The sudden appearance of the dc voltage at the inverter led to commutation failure of the inverter and therefore to a spike in the dc current at the rectifier. The net current is the combination of the line-charging current and the current in the inverter. As the dc line current was greater than the threshold current of the fault detection circuit, the protective control action was triggered, and the entire protection process repeated continuously. The test system could not recover at all for this protection scheme. There was no significant difference whether the dc filters or the 12-pulse system was used. The only difference was the amount of ripple on the dc voltage waveforms at both ends. Theoretically, the ripple of the dc voltage is minimum when a diode bridge rectifier is employed. The ripple of the dc voltage at the rectifier in the experiment was relatively high because of the generation of harmonics in the small synchronous generator model. Thus it can be concluded that this protection scheme will not work in practice.

5.3.2 AC voltage control with de-excitation and ac breaker

The results of the second protective scheme for 6-pulse operation without and with the dc filters are shown in Fig.5.5 and Fig.5.6 respectively. For the 12-pulse operation, the results are shown in Fig.5.7 . After the temporary fault was created, the control action was similar to the previous scheme. But in this case, a de-excitation voltage of amplitude -5 p.u. was applied to the field terminal of the generator. The field current, as well as the generated voltage, was reduced toward zero simultaneously. The dc currents also reached zero within 0.2 s. The ac breaker was reclosed and the field was magnetized 0.5 s later by the control. At this time, the ac voltage of the generator, which was reduced to a low level, did not cause an excessive overcurrent in the dc link. Therefore the system recovered from the fault within about 1.5 s. If the time duration for the field de-excitation, and consequently the time for opening the ac breaker, was made longer, there would be no spike in the dc current or the dc voltage at reclosing of the breaker. But the recovery time from the fault would be much longer. Thus this system worked properly as required for all system arrangements.

5.3.3 DC voltage control with ac breaker

Similar results obtained from the third protection scheme are shown in Fig.5.8, Fig.5.9 and Fig.5.10 . The only difference from the previous results is the waveform of the ex-

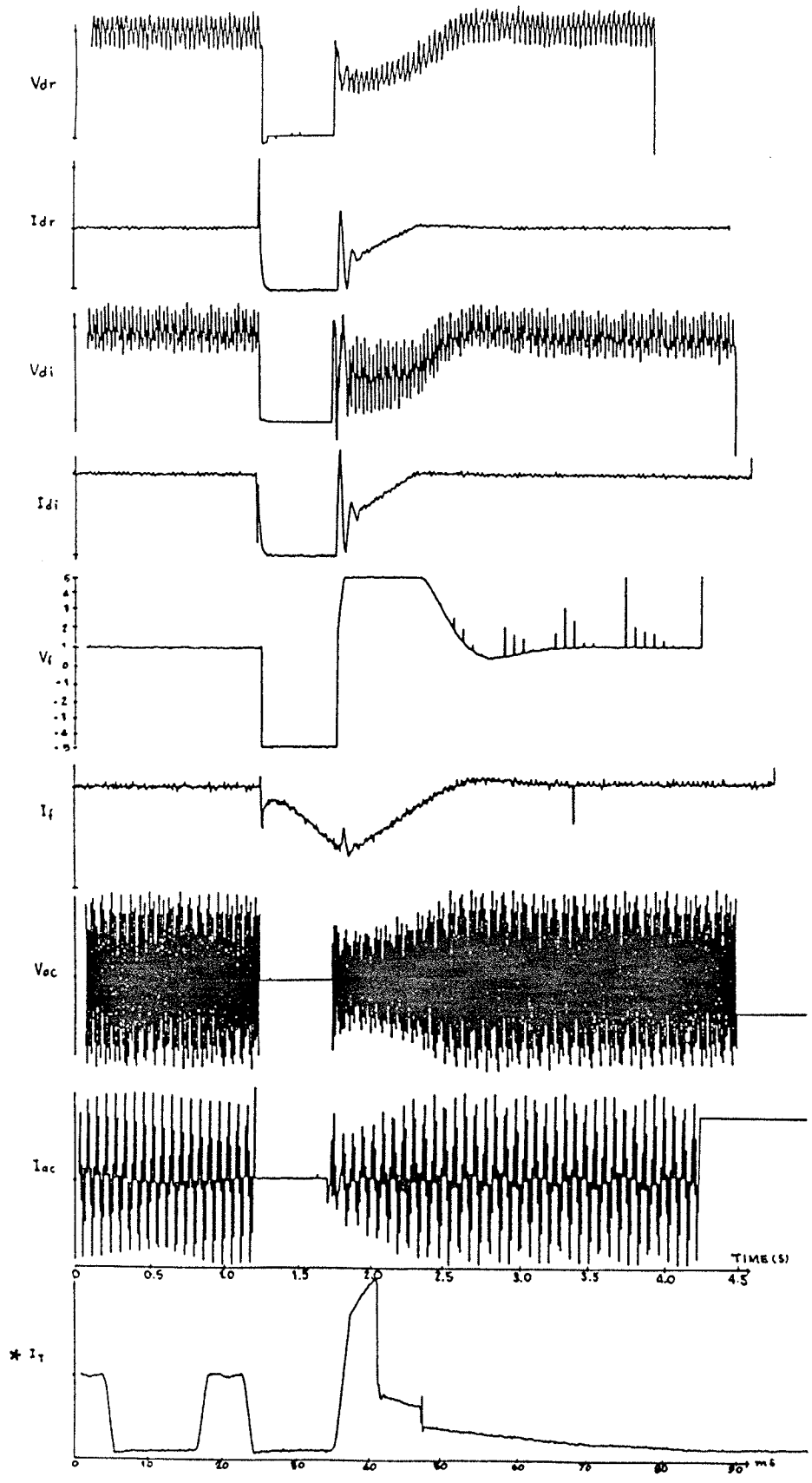

Figure 5.5: Response of scheme (b) for 6 pulse without dc filter

* one bridge arm current with enlarged time scale

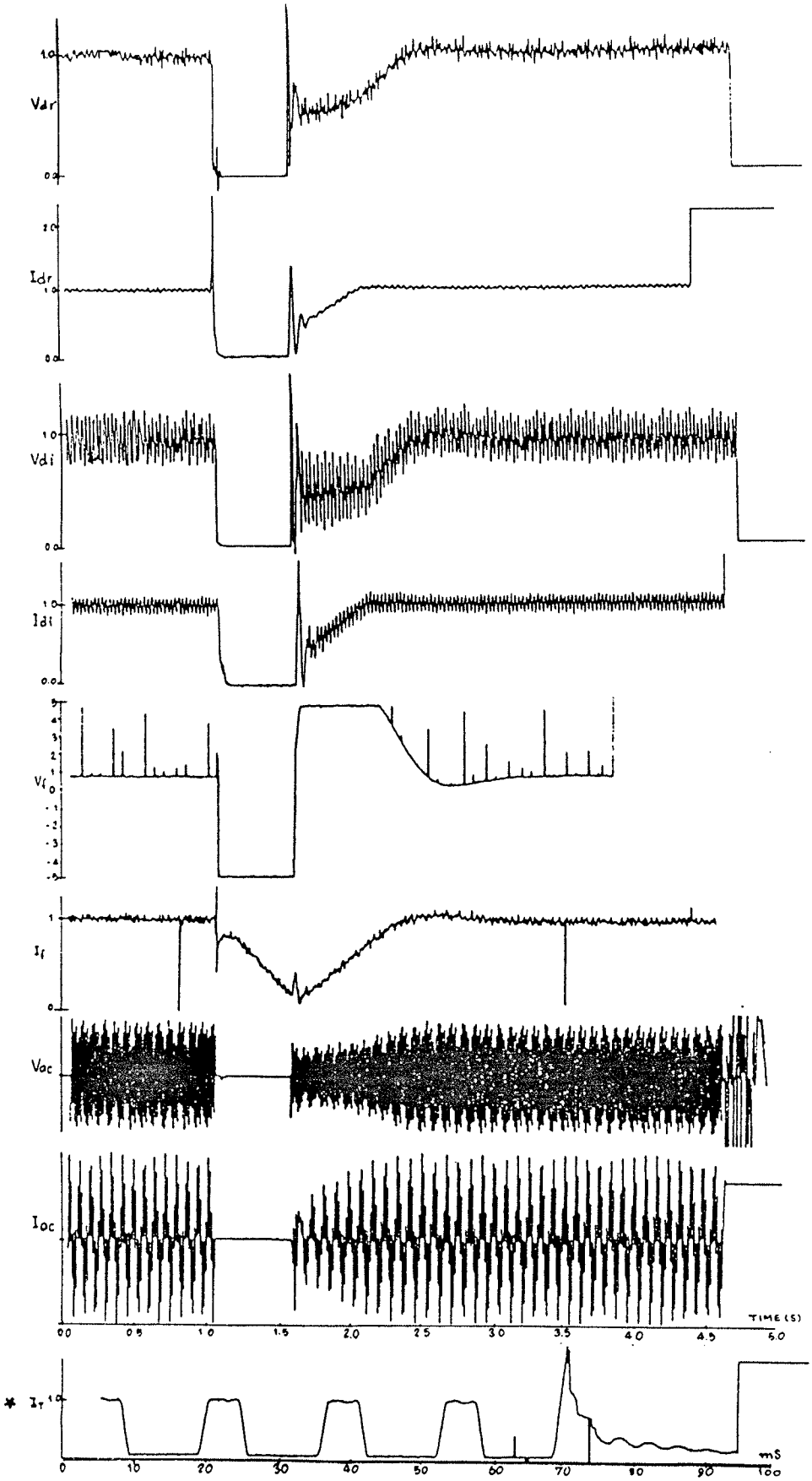

Figure 5.6: Response of scheme (b) for 6 pulse with dc filter

* one bridge arm current with enlarged time scale

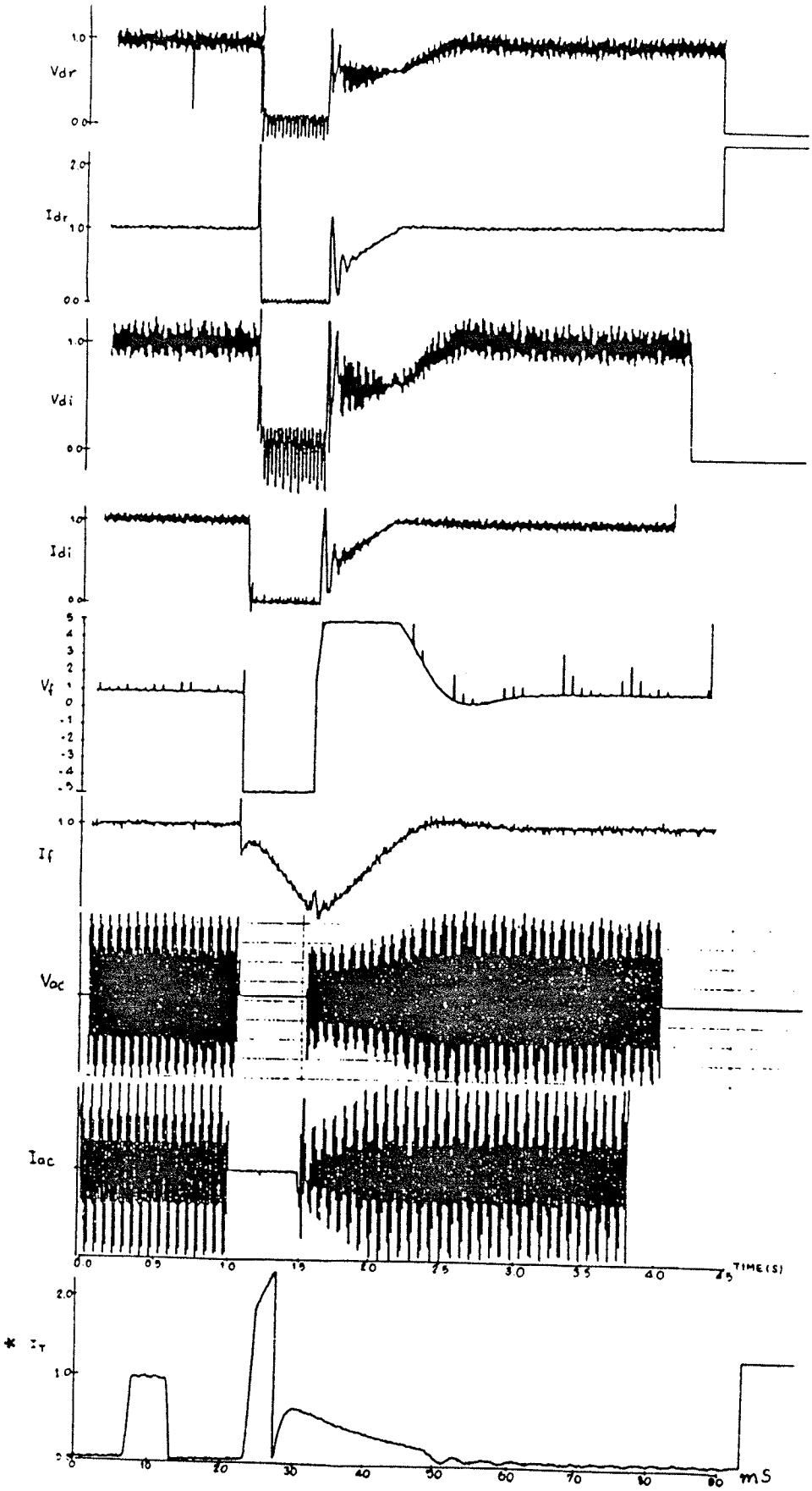

Figure 5.7: Response of scheme (b) for 12 pulse with dc filter

* one bridge arm current with enlarged time scale

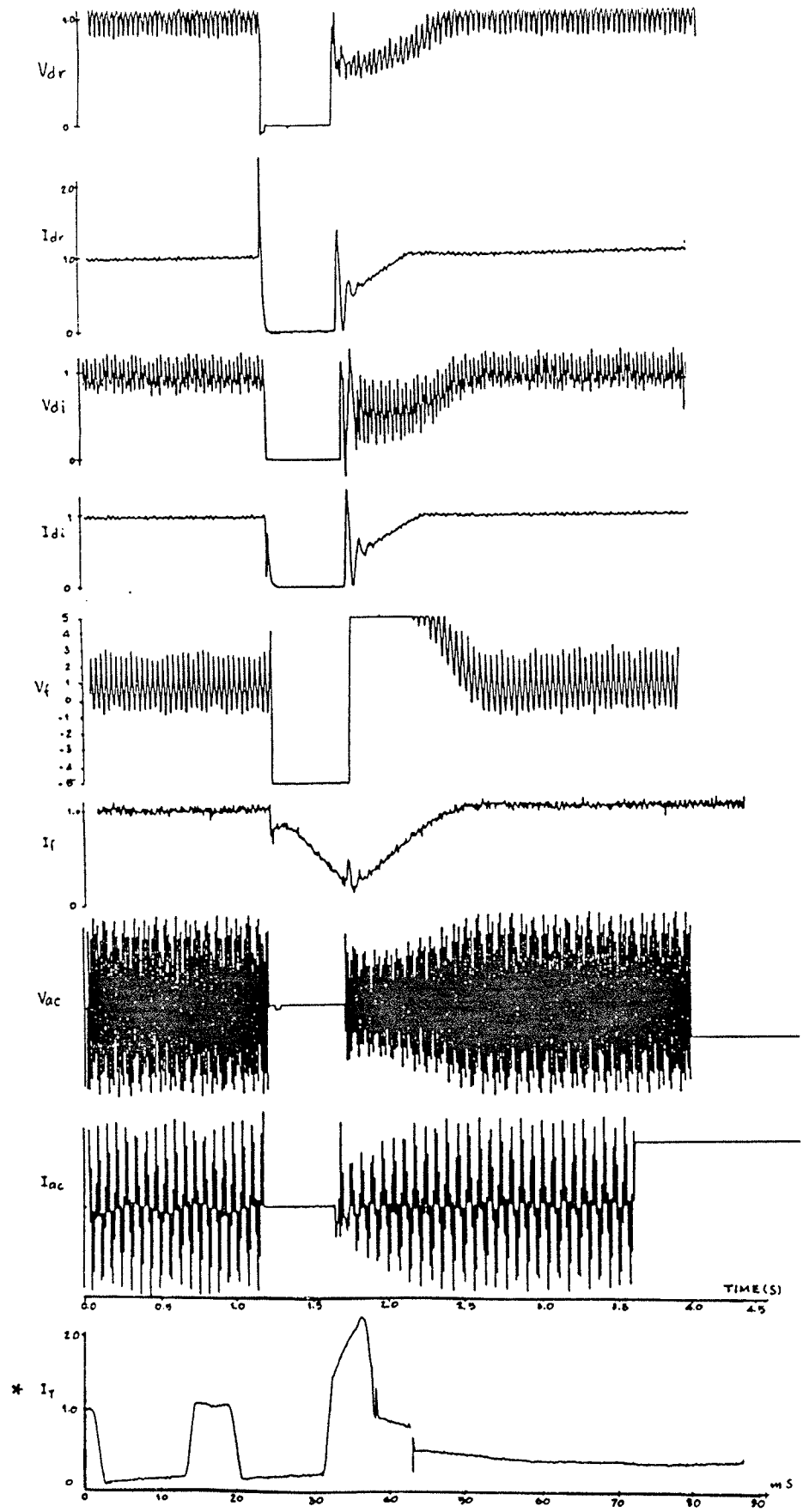

Figure 5.8: Response of scheme (c) for 6 pulse without dc filter

* one bridge arm current with enlarged time scale

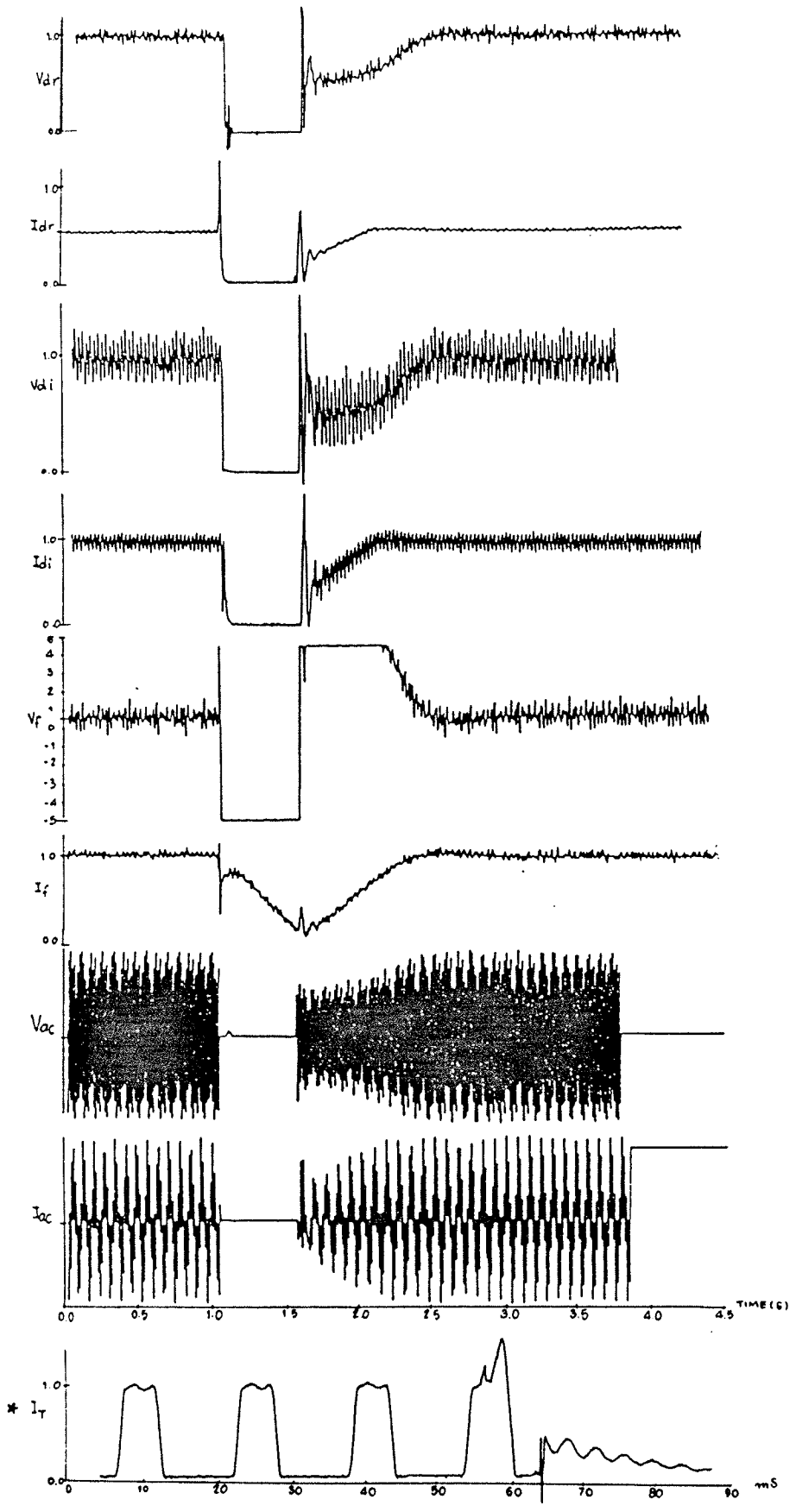

Figure 5.9: Response of scheme (c) for 6 pulse with dc filter

* one bridge arm current with enlarged time scale

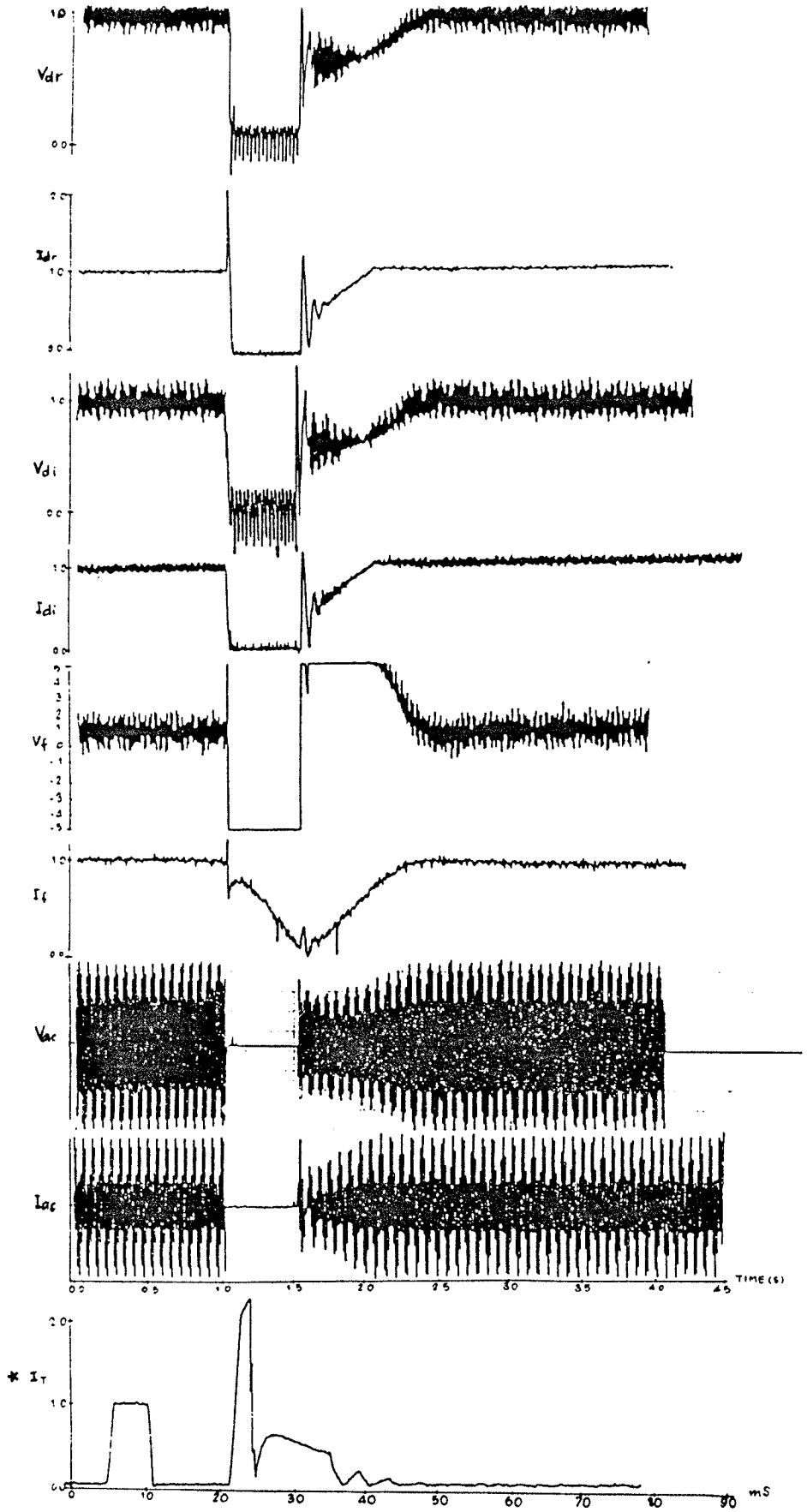

Figure 5.10: Response of scheme (c) for 12 pulse with dc filter

* one bridge arm current with enlarged time scale

citation voltage. In the previous scheme, the ac voltage was rectified and filtered with a large capacitor, and therefore less noise voltage was present at the output of the controller. But the ripple voltage of the excitation did not have any effect on the response of the system. Thus it was unnecessary to filter the dc voltage before it was fed into the controller. The system also recovered within 1.5 s after the line fault was created for all arrangements.

5.3.4 DC voltage control without ac breaker

The results of the last protection scheme are shown in Fig.5.11, Fig.5.12 and Fig.5.13 for all arrangements described earlier. The absence of an ac breaker prolonged the current in the dc link. The decay of the dc current followed the rate of decrease of the generator voltage which was determined by the field time constant (artificial time constant) and the reverse ceiling voltage of the generator. The peak of the dc current at the rectifier was about 2.5 p.u. and it took about 1.5 s to reduce the dc current to zero. Since the terminal voltage was reduced to a very low level, it took a very long time before the system restarted. The recovery time of this system was about 2.5 s. In this protection system, the diode rectifiers have to withstand an overload current for about 0.5 s (about 30 cycles). This period is quite long and the diodes may be destroyed. Had a diode with a higher current rating been selected, the advantage of economy would be lost. The peak dc current at the

inverter was also high because only a temporary fault was created. After the fault had been cleared, the dc current in the link continued flowing through the by-passed valves in the inverter. If a permanent line fault were created, the dc current at the inverter would decrease to zero very fast. In spite of its simplicity and economical advantage, this system is not attractive because it takes a long period of time to recover from the line fault.

5.4 DIGITAL SIMULATION

For further studies the system was also simulated digitally in time domain by using the EMTDC program available at the Department of Electrical Engineering. Only 12 pulse operation was simulated. A monopole 12 pulse HVDC system of rating 120 MVA, 150 kV, 556 mile dc line was considered. A temporary dc line fault was created at the middle of the line to study the effectiveness of the earlier described control strategies. A single isolated generator model was connected to the available thyristor bridge rectifier model. The thyristors of the rectifier bridge were forced to operate as diodes by setting their firing angles to zero. This technique might not represent the real diode characteristics because the firing angle of each thyristor is controlled relatively to the terminal voltage of the generator. Since the firing instant for the case of the diode rectifier must coincide with the internal voltage behind the subtransient reactance of the generator, therefore, the firing instant of

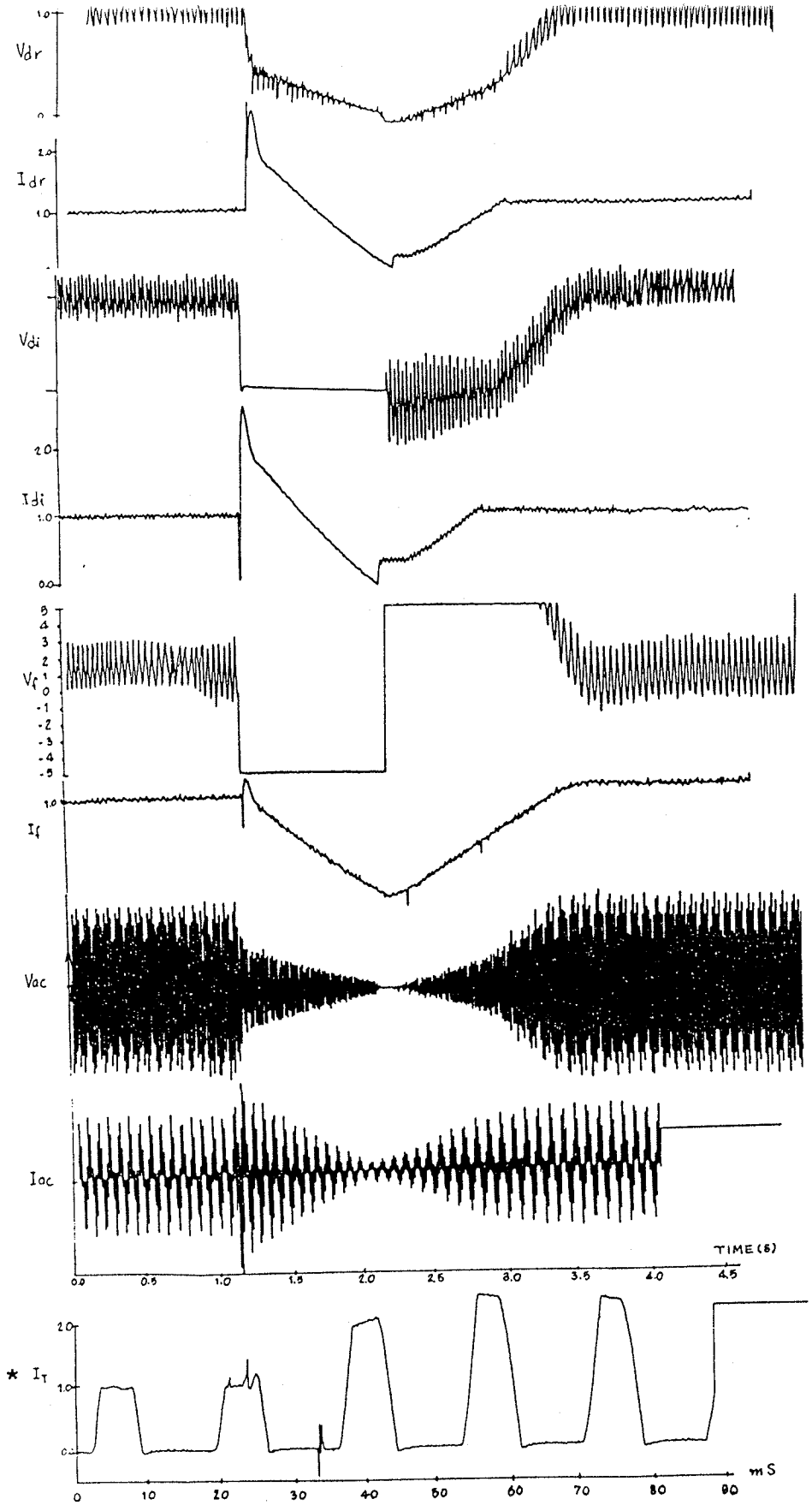

Figure 5.11: Response of scheme (d) for 6 pulse without dc filter

* one bridge arm current with enlarged time scale

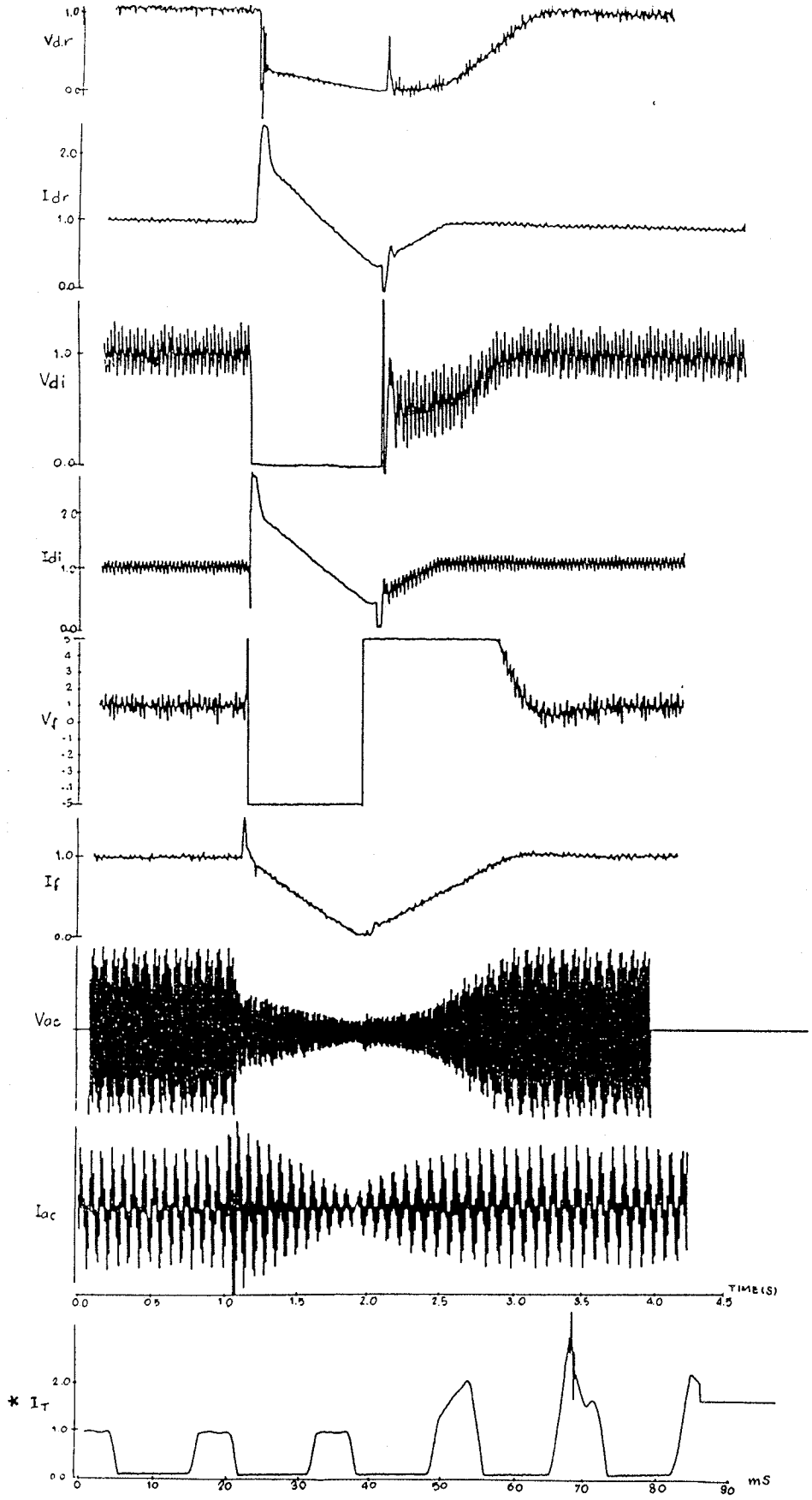

Figure 5.12: Response of scheme (d) for 6 pulse with dc filter

* one bridge arm current with enlarged time scale

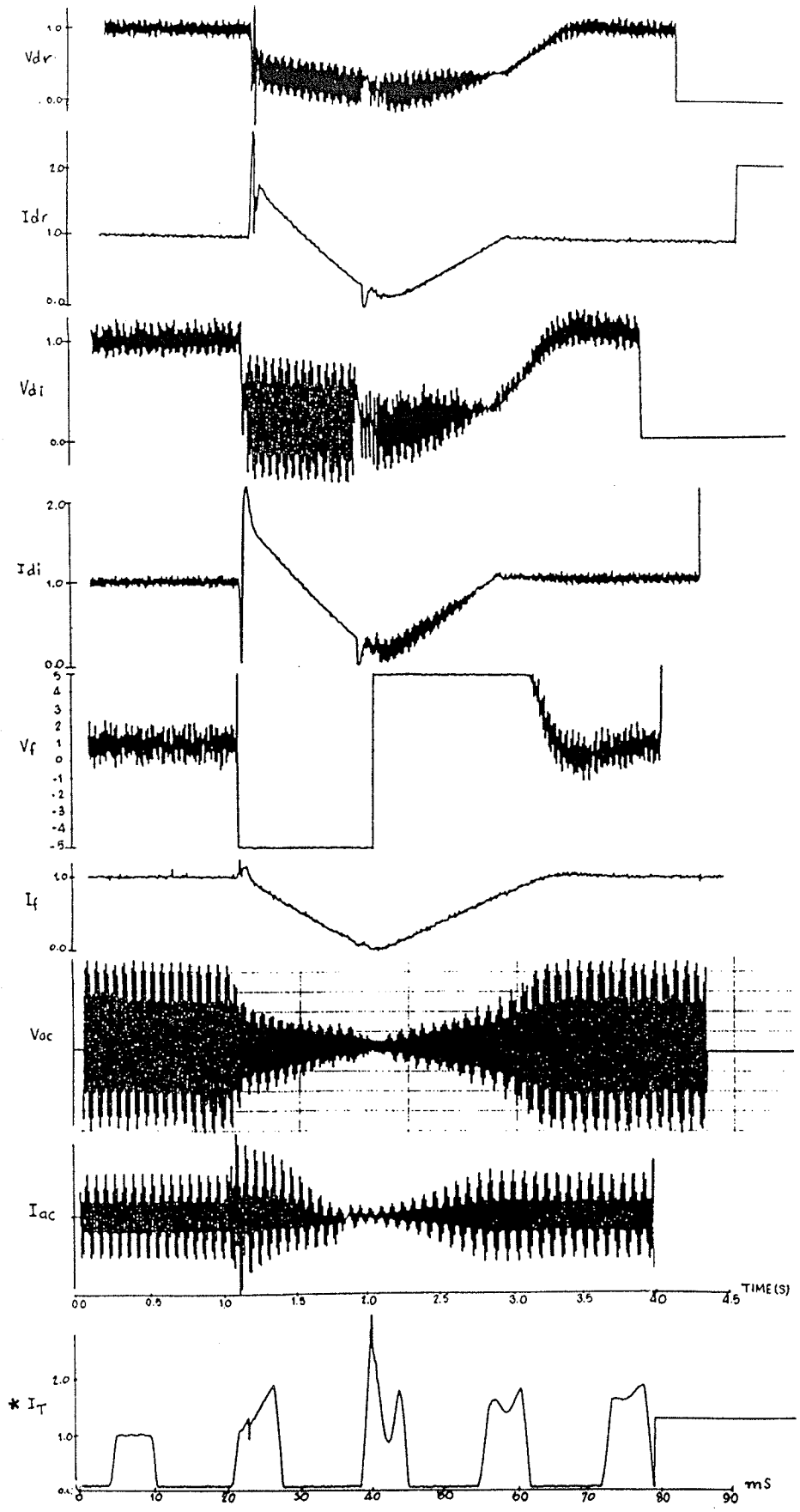

Figure 5.13: Response of scheme (d) for 12 pulse with dc filter

* one bridge arm current with enlarged time scale

the thyristor can not be made to coincide the firing instant of the diode rectifier even though the firing angle of the thyristor is zero. The firing instants of the diode and of the thyristor are shown in Fig.5.14 .

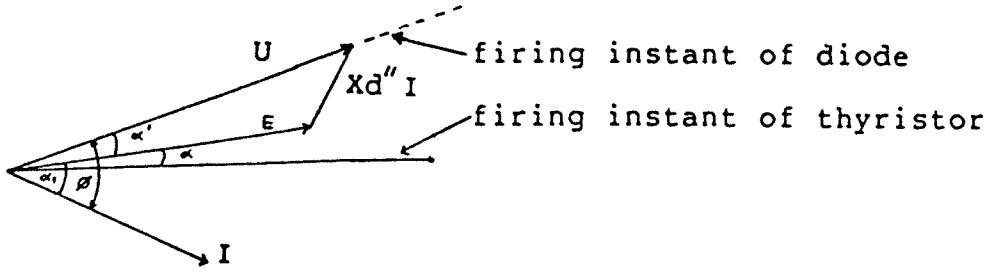

Figure 5.14: Diode and thyristor firing instant

The discrepancy of the firing instant is the angle α', which can be evaluated from the phasor diagram shown in Fig.2.9 . The angle α was found to be

$$\alpha' = \emptyset - \alpha_1$$
$$= 22.33 - 15.45$$
$$= 6.88\ ^\circ$$

The effect of the angle α' is that the ideal no-load voltage at the rectifier is dropped by 0.7% which can be neglected.

5.4.1 Digital simulation results

The response of the system for all protection schemes obtained from the digital simulation are shown in Figs.5.15 to 5.18 . They are relatively similar to those obtained from the experiment with the analog simulation. Controversially,

the protection scheme with ac voltage control and the application of the ac breaker did not cause an excessive overcurrent when the breaker was reclosed. The reason for this disagreement might be the difference in the transmission line model and the control characteristics of the inverter. In the analog simulation, distributed line parameters were not included in the model. A rapid increase in the dc voltage at the rectifier when the breaker was reclosed also resulted in a sudden rise of the voltage at the inverter without time delay. The rate of change of the dc voltage (dv/dt) at the inverter might be so high so that the thyristors were forced to conduct. This resulted in a very high current at the instant of the reclosing of the ac breaker. In the digital simulation, distributed parameters were included in the model. The dc voltage waveform at the inverter did not increase so fast due to the effect of the distributed line model. The pulse voltage was also absorbed and delayed in the transmission line. Thus self firing of the thyristor at the inverter did not occur. The waveforms of the dc voltages and of the dc currents from the digital simulation are shown in Fig.5.15 . Thus this system offered the fastest recovery time. However the voltage stress on the thyristor valve might deteriorate the life of the thyristor. The response of the dc voltages and of the dc currents from this simulation differed somewhat from the the results achieved from the analog simulation. The response were oscillatory after the the temporary fault was cleared. The cause of this phenomenon

might be the effect of the distributed line parameters. The results of digital simulation with field de-excitation and with the application of the ac breaker are shown in Fig.5.15 and Fig.5.16 . The system recovered within 1.8 s. The recovery time was so long due to the fact that the field current was reduced to zero before the reclosing of the ac breaker. Without the application of the ac breaker, the system also recovered within about 1.8 s. In all cases. the peak dc currents were found to be about 3.0 p.u., which was slightly higher than that of the analog simulation. There were some basic differences in the responses obtained from analog and digital simulations some of which may be on account of the dc line representation.

5.5 SUMMARY

1. Analytical expressions for the transfer functions of the machine and the converter were derived and were presented.
2. An artificial time constant was added to the control circuit to represent a practical generator.
3. A lead compensator was designed to increase the system stability and to improve the system response.
4. An isolating dc voltage transducer was designed for the purpose of dc voltage control in the dc link.
5. A diode bridge rectifier in unit connection with a generator was set up on the physical component real

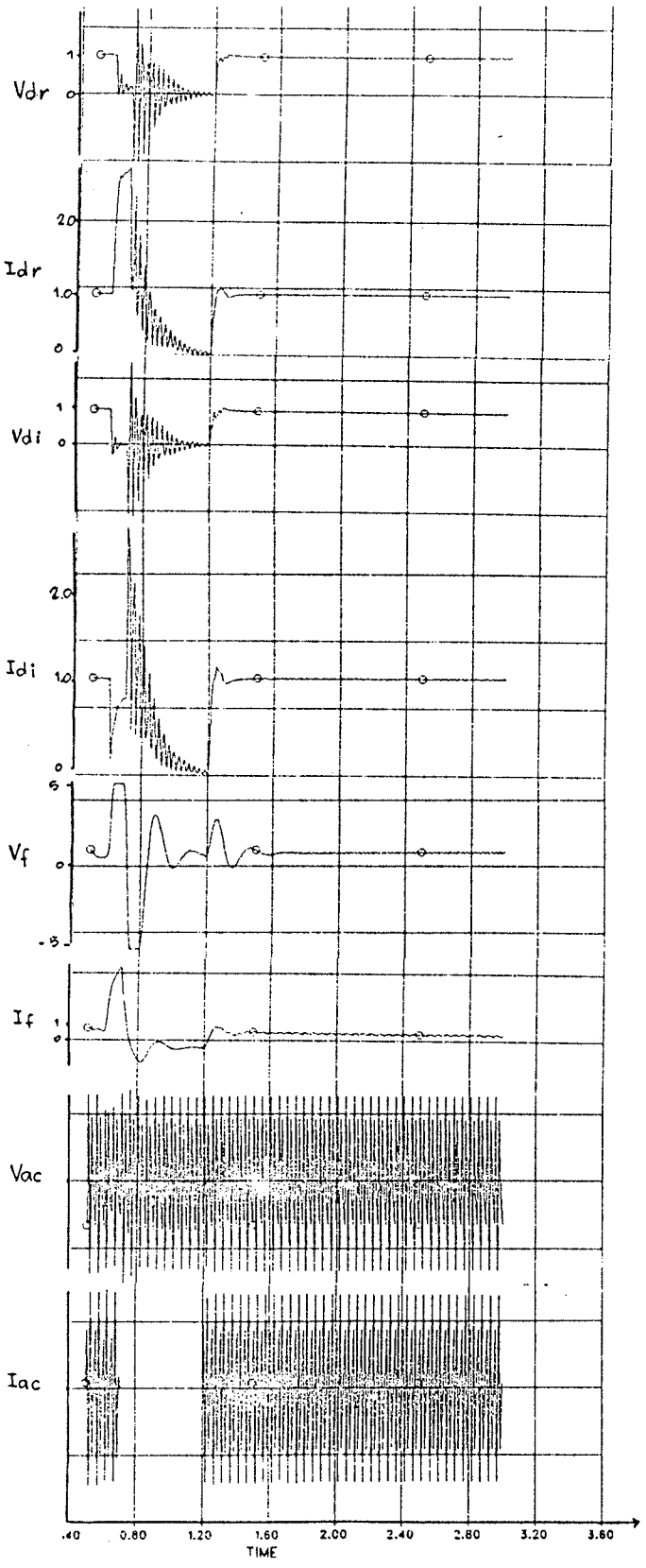

Figure 5.15: Response of scheme (a) from digital simulation

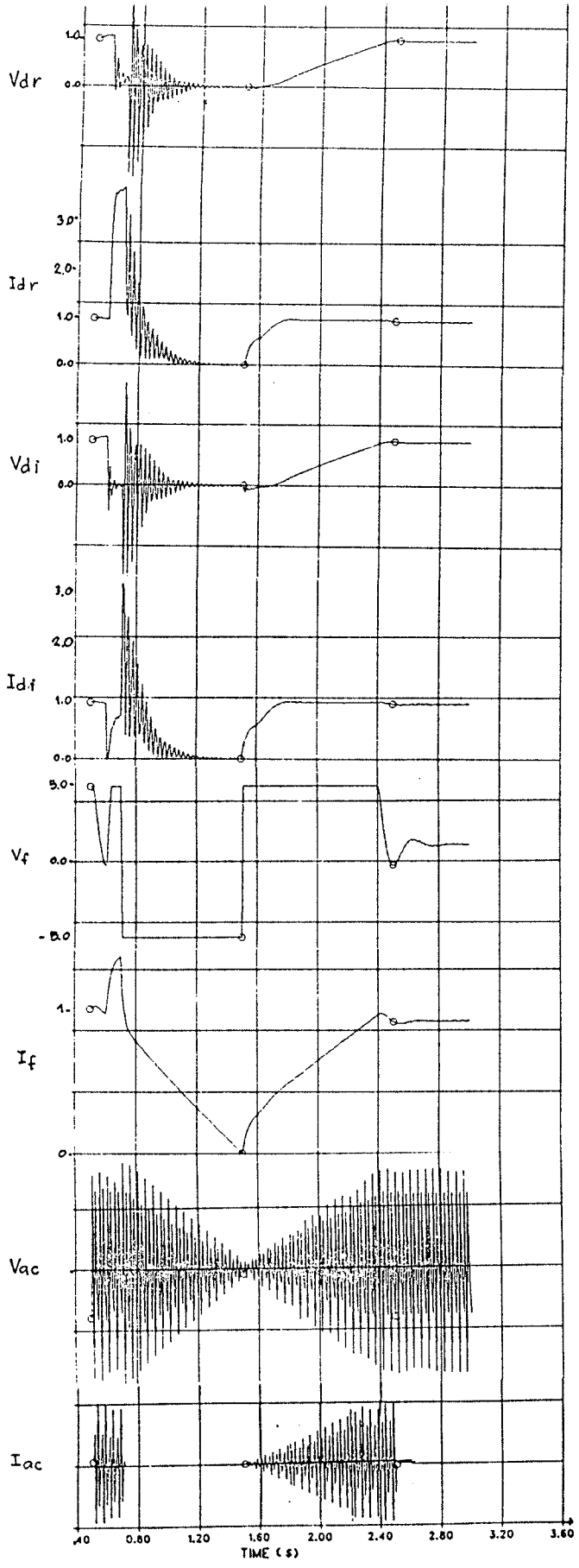

Figure 5.16: Response of scheme (b) from digital simulation

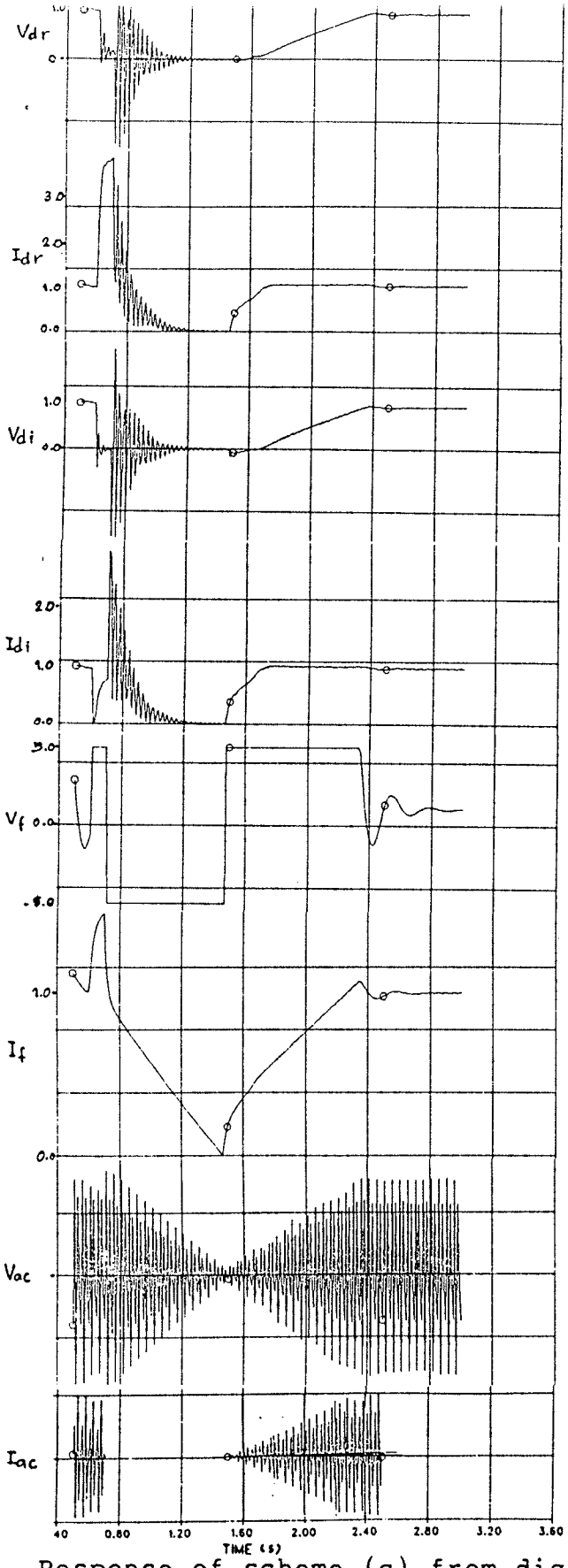

Figure 5.17: Response of scheme (c) from digital simulation

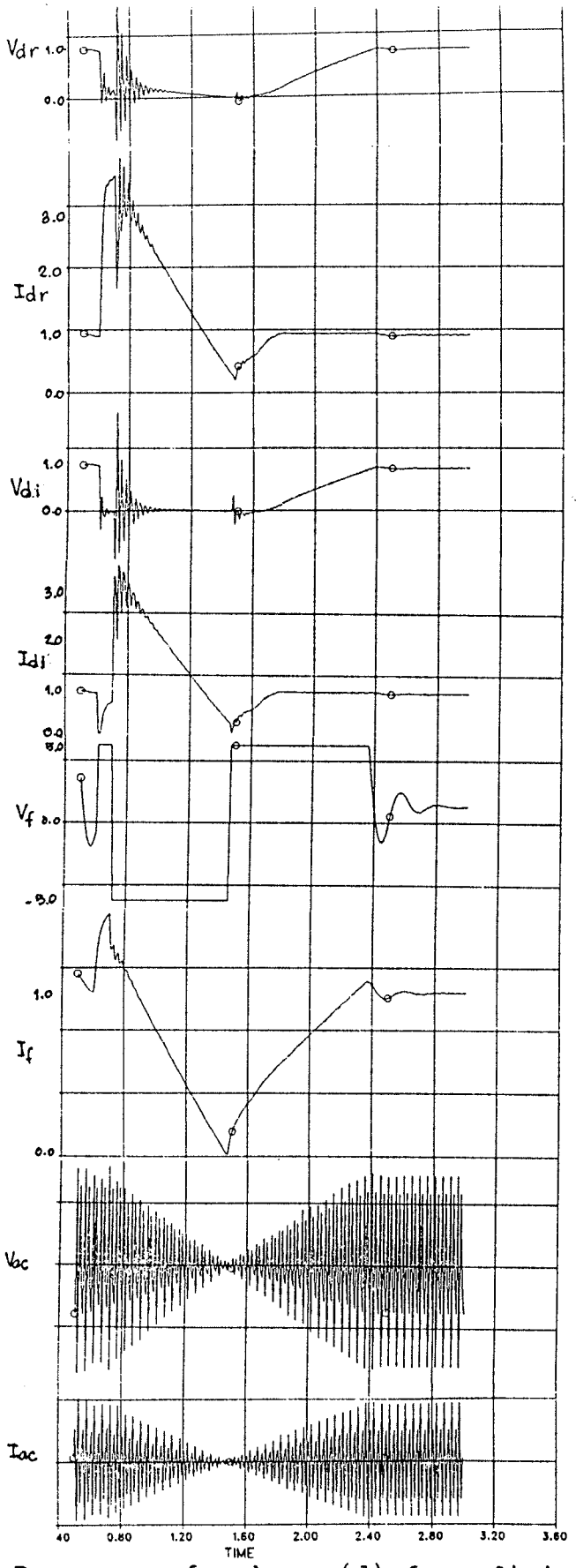

Figure 5.18: Response of scheme (d) from digital simulation

time simulator for evaluating different protection and restart schemes.

6. Digital simulation of a system with a long dc line was performed by using the EMTDC program.

5.5.1 Problems encountered in digital simulation and their resolution

One of the problems encountered with the digital simulation was the instability of the synchronous generator model of the EMTDC program. The model was orginally developed for interfacing the generator to the EMTDC system. The machine was modeled as a current source feeding an ac network in the EMTDC program. In the simulated system, the ac breaker was required to disconnect the generator from the ac system. Once the breaker was opened, the operation of the machine collapsed. Theoretically, a current source can not be open-circuited. To avoid this problem, the generator was terminated with proper resistance. If the resistance was too high the problem could not be resolved. On the other hand, if the resistance was too low, the machine was loaded by the resistors. Another problem was the diode bridge rectifier simulation. As mentioned earlier, the thyristor bridge rectifiers were forced to conduct at the the firing angle of 0° to represent the diode operation. In addition to the problem that the actual firing angle could not be made exactly zero relative to the internal commutation voltage, the synchronization of the firing pulses with the ac voltage at the recti-

fier was also a problem. Since the generator was connected to the rectifiers without ac filters to reduce the cost of the system, the ac voltage waveform was no longer sinusoidal while the system was operating. Therefore, the synchronization of the firing pulses, which was obtained from the zero crossing routine in the EMTDC program, was unstable. This resulted in random shifting of the firing pulses. If a diode bridge rectifier model were available in the EMTDC program this problem would not happen as no firing pulses were required.

5.6 DISCUSSION AND CONCLUSION

Whether or not a unit connected diode rectifier can be used in reality is an interesting question. From the economical point of view, the system offers a reduction in the cost of the rectifier, protective switches, ac busbar, filters, etc. But it has to be compensated with the cost of ac breaker or dc breaker and the additional cost of the higher reactive power consumed at the inverter. Fast communication between the rectifier and the inverter is not essential because the dc line fault can also be detected at the inverter. Once the fault is detected, the thyristors at the inverter can be blocked, by-passed and the current setting can be ramped up after a predetermined time by its own controller. On the whole, the system may be cheaper when the ac breaker or low interrupting capacity dc breaker is employed.

From the technical point of view, the system works perfectly as in the case of the conventional system in normal operation. But in the case of dc line fault or fault at the inverter, the total system collapses for a longer period of time. As the recovery time from fault of the system can not be made too fast, system instability at the receiving end may occur if the capacity of the dc system is comparable to ac system capacity at the receiving end. The instability would be caused due to a large loss of energy input. In order to get around this problem, some loads connected at the receiving end must be tripped for a short period required for clearing the dc line fault. On a smaller scale, if the power is transmitted solely from a remote generator to a certain area, a synchronous generator is required at the inverter station. The capacity of the synchronous generator must be made large enough so that it can supply the emergency loads in that area at the occurrence of dc line fault.

If the receiving end is fed by many HVDC links, this problem is not so serious. The problem can be resolved by increasing the transmitted power at each station as soon as one dc link collapses. Because of the fast controllability of the systems, this action can be taken in a very short time.

The main disadvantage of this scheme relates to the clearing of dc line fault. The power recovery is comparatively slow. Therefore it can be concluded that the diode

bridge scheme could be a realistic economic alternative if fast recovery from dc line fault and reversal of power are not required.

BIBLIOGRAPHY

[1] Adkins B,'The General Theory of Electrical Machine', London : Chapmann and Hall, 1962.

[2] Clark E,'Circuit Analysis of AC power system Vol II', New York : Wiley,1943-1950.

[3] Bolwes J.P.,'HVDC System Development and Concepts : The diode Rectifier', CIGRE study committee 14, Meeting & Colloquium, Winnipeg, Canada, June 1977.

[4] Ryczkowski E.M.,'Some Compensation Techniques applied to a Laboratory Power System',MSc Thesis ,University of Manitoba , 1977 .

[5] Clade' J.J and Persoz H., ' Calculation of Dynamic Behavior of Generators connected to a d.c. link ' IEEE Trans ,PAS-89 , pp 1553-1564 , 1968 .
IEEE Trans, PAS-89,

[6] Machida T. and Ishikawa I .,' Control and Protection Systems for dc Transmission System with Diode valve Converter ', IEEE International Semiconductor power converter conference,Orlando/Florida, USA,March 1977.

[7] Hausler M. and Kangiesser K.W .,' Generator-converter Unit Connection with Thyristor and Diode Rectifiers', Conference Incorporating HVDC power transmission into system planning ',Phoenix, March 1980 .

[8] Arrillaga J.,'High Voltage Direct Current Transmission', London : Pereginus, 1983 .

[9] Kimbark E.W. ,' Direct Current Transmision Vol I ', New York : Wiley , 1971 .

[10] Adamson C. and Hingorani N.G., ' High Voltage Direct Current Power Transmission ' , London : Garraway ,1960.

[11] Ogata K.,'Modern Control Engineering',Prentice-Hall,1976.

[12] Shinners S.M.,'Modern Control System Thoery and Application' London : Addison-Wesley , 1978.

[13] Nagrath I.J. and Gopal M.,'Control Systems Engineering', New York : Wiley , 1975.

[14] Sugandhi R.K. and Sugandhi K.K.,'Thyristors: Theory and Application', New York : Wilely 1981.

[15] Design of back to back system model, HVDC system simulator, University of Manitoba Canada.

Appendix A

SYSTEM TRANSFER FUNCTION REDUCTION

Generator transfer function simplification :

From the equation (2.36)

let $k_1 = \sin\emptyset u \cos\emptyset u \tan(\emptyset+\theta')$

$k_2 = \tan^2(\emptyset+\theta')$

$k_3 = \frac{\rho'}{\cos\theta'}$

$k_4 = \rho'\cos\theta \;/\; \rho\cos\theta'$

This equation will be simplified to be

$$\frac{\Delta U}{\Delta Ef} = \frac{k_3 G(p)(k_5+k_1)}{1+\frac{k_1}{k_2}(1+(k_4+k_3)F(p)-k_4+k_2)} \qquad (A1)$$

$$= \frac{G(p)k_3(k_5+k_1)}{1+\frac{k_1}{k_2}(1+k_2-k_4+(k_4-k_3)F(p))} \qquad (A2)$$

again let

$m_1 = k_3(k_5+k_1)$

$m_2 = k_1/k_2$

$m_3 = 1+k_2-k_4$

$m_4 = k_4-k_3$

equation (A1.2) can be simplified further to

$$\frac{\Delta U}{\Delta Ef} = \frac{G(p)\ m_1}{1+m_2(m_3+m_4F(p))} \qquad (A3)$$

$$= \frac{G(p)\ m_1}{1+m_2\left[m_3+m_4.\frac{1+Td'\ p}{1+Tdo'p}\right]}$$

$$= \frac{G(p)\ m_1}{1+m_2\left[\frac{m_3+Tdo'm_3p+m_4+m_4Td'p}{1+Tdo'\ p}\right]}$$

$$= \frac{G(p)\ m_1\ (1+Tdo'\ p)}{1+m_2m_3+m_2m_4+((1+m_2m_3)Tdo'+m_2m_4Td')p}$$

$$= \frac{m_1}{1+m_2(m_3+m_4)}G(p)\frac{1+Tdo'p}{1+Td*\ p}$$

$$Td* = \frac{(1+m_2m_3)Tdo'+m_2m_4Td'}{1+m_2(m_3+m_4)}$$

substitute m backward for k yield

$$\frac{\Delta U}{\Delta Ef} = G(p)\frac{(k_3(k_1+k_5))}{1+\frac{k_1}{k_2}(1+k_2-k_4+k_4-k_3)}\ \frac{1+Tdo'\ p}{1+Td*\ p}$$

$$= \frac{k_3(k_1+k_5)}{1+\frac{k_1}{k_2}(1+k_2-k_3)}G(p)\ \ \frac{1+Tdo'p}{1+Td*\ p}$$

$$= K_m\ \ G(p)\ \ \frac{1+Tdo'p}{1+\ Td*p}$$

$$Km = \frac{\rho'}{\cos\theta'}\ \frac{(\ \sin\phi u\ \cos\phi u\ \tan(\theta'+\phi)\ +\ \cos^2\theta')}{1+\frac{\sin\phi u\ \cos\phi u}{\tan(\theta'+\phi)}\ (1+\tan^2(\theta'+\phi)-\frac{\rho'}{\cos\theta'})}$$

and

$$Td^* = \frac{1+\frac{k_1}{k_2}(1+k_2-k_4)Tdo' + \frac{k_1}{k_2}(k_4-k_3)Td'}{1+\frac{k_1}{k_2}(1+k_2-k_4+k_4-k_3)}$$

$$= \frac{1+\frac{k_1}{k_2}(1+k_2-k_4)Tdo' + \frac{k_1}{k_2}(k_4-k_3)Td'}{1+\frac{k_1}{k_2}(1+k_2-k_3)}$$

$$= \frac{1+0.5\sin 2\phi_u\left(\cot(\phi+\theta')\left(1-\frac{\rho'\cos\theta}{\rho\cos\theta'}\right)+\tan(\phi+\theta')T_{do'}+\frac{0.5\sin 2\phi_u}{\tan(\phi+\theta')}\left(\frac{\rho'}{\rho}\frac{\cos\theta}{\cos\theta}-\rho\right)\right)Td'}{1+0.5\sin 2\phi_u\left(\cot(\phi+\theta')\left(1-\frac{\rho'}{\cos\theta'}\right)+\tan(\phi+\theta')\right)}$$

Appendix B

FIELD CURRENT REDUCTION

Reversed voltage application

Assume that a current Io is flowing in a field winding having resistance R and inductance L under the applied voltage V. At time t=0,a reverse voltage of magnitude V.Nv,where Nv is the reverse voltage factor, is suddenly applied to the winding. The current in the winding can be derived as shown;

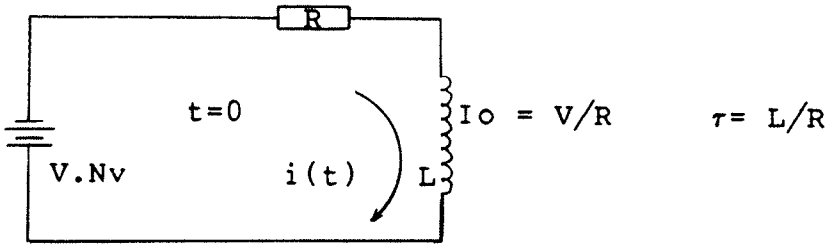

$$-V.Nv = Ri(t) + L\frac{di(t)}{dt}$$

apply Laplace transform to get

$$-\frac{V.Nv}{s} = RI(s) + sLI(s) - LIo$$

$$I(s) = \frac{Io}{s+R/L} - \frac{1}{L}\frac{V.Nv}{s(S+R/L)}$$

$$= \frac{Io}{s+R/L} - \frac{V.Nv}{R}\left(\frac{1}{s} - \frac{1}{s+\tau}\right) \qquad (B1)$$

$$i(t) = Io\, e^{-t/\tau} - Io(1-e^{-t/\tau})$$

$$\frac{i(t)}{Io} = (1+Nv)\, e^{-t/\tau} - Nv \qquad (B2)$$

Damping resistance application

Holding the previous assumptions at time t=0, a damping resistance R.Nr, where Nr is the ratio of the damping resistance to the resistance of the field winding, is connected in parallel to the terminal of the field winding. The equation (B1) can be used to determine the current by setting V=0 and R'=R+R.Nr .

from (B1)

$$I(s) = \frac{Io}{s+R'/L}$$

$$= \frac{Io}{s+\tau'}$$

$$i(t) = Io\, e^{-t/\tau'}$$

$$\frac{i(t)}{Io} = e^{-(1+Nr)\,t/\tau} \qquad (B.3)$$

Appendix C

LEAD COMPENSATION DESIGN

Once the location of the compensated pole-zero is known, the circuit shown in figure C1 can be used .

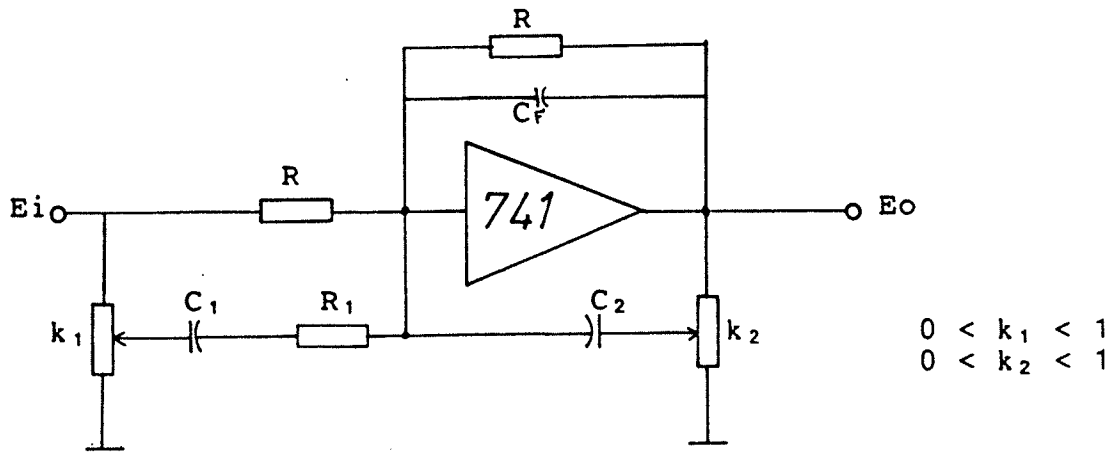

Figure C.1: Lead compensation circuit

Assume that there is no loading effect on the amplifier,

$$Ei\left[\frac{1}{R}+\frac{k_1}{R_1+1/sC_1}\right]=-Eo\left[\frac{1}{R}+\frac{1}{1/sC_F}+\frac{k_2}{1/sC_2}\right] \quad (C1)$$

$$Ei\left[\frac{(1+sR_1C_1)+sk_1RC_1}{R(1+sR_1C_1)}\right]=-Eo\left[\frac{1+s(k_2RC_2+RC_F)}{R}\right]$$

$$\frac{Eo}{Ei}=\frac{1+a(k_1RC_1+R_1C_1)}{(1+sR_1C_1)[1+s(k_2RC_2+RC_F)]}$$

$$= \frac{1+s(T_A + T_B)}{(1+sT_B)(1+s(T_C + T_D))} \qquad (C2)$$

where

$T_A = k_1RC_1$ (lead time constant)

$T_B = R_1C_1$ (noise filter time constant)

$T_C = k_2RC_2$ (lag time constant)

$T_D = RC_F$ (amplifier stabilizing time constant)

If the noise bandwidth and the bandwidth of the amplifier are limited to be only 100 Hz and 1kHz respectively, the valur of T_B and T_D should be

$T_B = 0.01$ s.

$T_D = 0.001$ s.

Assume that the desired pole-zero location is at

Zc = -10 => $(T_A + T_B) = 0.1$ s.

Pc =-100 => $(T_C + T_D) = 0.01$ s.

then $T_A = 0.09$ s.

$T_C = 0.009$ s.

The optimum value of k_1 and k_2 should be 0.5 in order to be able to adjust the position of pole-zero experimentally.

Therefore;

$RC_1 = T_A/k_1 = 0.18$ s.

$RC_2 = T_C/k_2 = 0.018$ s.

if C_1 is chosen to be 1 μF, then

R = 180 Kohm , C_1 = 0.1 μF

R_1 = 10 Kohm and C = 5 nF